

# MICROFLUIDIC PRODUCED LIQUID CRYSTALLINE SHELLS

Self-assembled structures in nematic and smectic shells

Dissertation zur Erlangung des Grades  
DOKTOR der NATURWISSENSCHAFTEN

im Promotionsfach Chemie

am Fachbereich Chemie, Pharmazie und Geowissenschaften

der Johannes Gutenberg-Universität Mainz

vorgelegt von

**HSIN-LING LIANG**

geboren in Taipei, Taiwan

Mainz 2013





**Doctoral Dissertation**  
**Institute of Organic Chemistry**  
**Johannes Gutenberg-University Mainz**

**Supervisors:**

Prof. Dr. Rudolf Zentel  
Organic Chemistry, Johannes Gutenberg-University Mainz

Prof. Dr. Jan P. F. Lagerwall  
Graduate School of Convergence Science and Technology and Advanced Institutes of  
Convergence Technologies, Seoul National University

**Dean:**

**Dissertation Committee:**

**Date of defence:** 25.09.2013



# Microfluidic Produced Liquid Crystalline Shells

*Self-assembled structures in nematic and smectic shells*

**Hsin-Ling Liang**

Institute of Chemistry

Johannes Gutenberg-University Mainz

## ABSTRACT

Liquid crystals exhibit reduced symmetry on cooling from the simple liquid state and organize themselves into a preferential direction. Attributed to the property of partial ordering while maintaining a certain degree of molecular mobility, they possess unique optical, electrical and mechanical performance. In the flat geometry, as in display panels, uniform and defect-free liquid crystalline alignment can be achieved. However in curved and closed geometries, *e.g.* in a sphere, the broken symmetries can yield definite total defect strength. As defects in liquid crystals are stabilized in dimensions of the visible range, the spherical form of droplets and shells serves as an ideal model for direct observations of topological singularities. Alongside being of interest on a fundamental level, colloidal liquid crystals with well-defined molecular orientation have been proposed for various modern applications, such as improved display modules by the polymer-dispersed-liquid-crystal (PDLC) system, dispersion of biodetectors, photonic colloidal crystals and miniaturized actuators from liquid crystalline elastomers.

The first objective of this thesis work was to construct microfluidic devices allowing for the production of shells from different liquid crystal materials. We investigated the influence of surface alignment on defect arrangement in shells from low molar mass liquid crystals, the alignment of which was controlled by the surface adsorption of anchoring agents. The investigation dealt with phase transition behavior and textual configurations in the nematic, smectic-A and smectic-C ordering subjected to different surface anchoring conditions. Moreover, the use of controlled orientation was presented in elastomeric liquid crystal shells. We fabricated core-shell liquid crystalline elastomers via photopolymerization in the microfluidic flow, where the orientation of the reactive mesogens was ensured by the flow shear stress. We examined the shape change of the elastomer shells upon actuation as a consequence of the uniformity of alignment.

For low molar mass shells, we found that in shells under planar alignment a buckling texture developed on the nematic to smectic-A transition, which was expected to be caused by smectic layer undulation triggered by the curvature strain of the shell morphology. We also explained the formation of rich focal conic domains in smectic-A shells under incompatible alignment on the two surfaces. A peculiar alignment transformation upon temperature changes was observed in shells decorated by polymeric surfactants F127, the process of which was discussed based on the change of textural configurations. Furthermore, we showed the first observation of smectic-A to -C transition in shells under homeotropic alignment. Finally, liquid crystalline elastomer shells with uniform nematic orientation were fabricated, and the unique actuating behavior of the shell volume was demonstrated as a heart-like micropump.

**Keywords:** liquid crystals, liquid crystalline elastomer, nematic shell, smectic shell, core-shell particle, micropump, double emulsion, capillary microfluidic device



# Mikrofluidische Herstellung von flüssigkristallinen Schalen

*Selbstorganisierende Strukturen in nematischen und smektischen Schalen*

Hsin-Ling Liang

Institut für Organische Chemie, Johannes Gutenberg-Universität Mainz

## ZUSAMMENFASSUNG

Beim Abkühlen aus der Schmelze nehmen Flüssigkristalle einen Zustand erniedrigter Symmetrie ein und organisieren sich entlang einer Vorzugsrichtung. Der Erhalt der kristallinen Fernordnung kombiniert mit der molekularen Beweglichkeit von Flüssigkeiten bewirkt einzigartige optische, elektrische und mechanische Eigenschaften. In einer flachen Geometrie, wie man sie zum Beispiel bei LC-Displays vorfindet, können homogene und defektfreie Anordnungen der Flüssigkristalle erhalten werden, während die gekrümmte und geschlossene Geometrie einer Kugel zwangsläufig zu Defekten führt. Da die Größenordnung der Defekte in einer flüssigkristallinen Matrix im sichtbaren Bereich ist, können kugelförmige Tropfen und Schalen aus Flüssigkristallen als ideales Modell zur Beobachtung von topologischen Singularitäten genutzt werden. Neben diesem grundlegenden Interesse bieten sich kolloidale Flüssigkristalle mit einer definierten molekularen Orientierung auch für verschiedene moderne Anwendungen an, wie verbesserte Anzeigemodule bei PDLC-Displays (polymer-dispersed liquid-crystal), Dispersionen für Biodektoren, photonische kolloidale Kristalle und miniaturisierte Aktoren aus flüssigkristallinen Elastomeren. Das Ziel dieser Arbeit war es, eine mikrofluidische Apparatur zu konstruieren, mit welcher sich Schalen aus verschiedenen flüssigkristallinen Materialien herstellen lassen. Der Einfluss der Oberflächenstruktur auf die Defektanordnung in Schalen aus niedermolekularen Flüssigkristallen wurde untersucht. Die Oberflächenstruktur wurde durch Adsorption von oberflächenaktiven Substanzen an die Grenzfläche beeinflusst. Das Phasenverhalten und die Texturen der unterschiedlichen Konfigurationen in den nematischen, smektisch A und smektisch C-Phasen wurden für verschiedene Oberflächen-Verankerungszustände beobachtet. Des Weiteren wurde das Konzept der kontrollierten Orientierung auf flüssigkristalline Elastomer-Schalen übertragen. Hier wurden Kern-Schale Systeme mittels photo-initiiertes Polymerisation erzeugt, wobei die einheitliche Orientierung der reaktiven Mesogene durch die Scherkräfte des umgebenden Flussfeldes erzeugt wurde. Infolge dieser einheitlichen Orientierung zeigten die Elastomer-Schalen beim Phasenübergang eine Formänderung. Für Schalen aus niedermolekularen Flüssigkristallen wurde im Fall einer planaren Orientierung eine Wölbung der Textur beim nematisch-smektischen Phasenübergang beobachtet, die durch eine Wellenbewegung der smektischen Schicht entsteht. Ursache dafür ist die durch die kugelförmige Form verursachte räumliche Beschränkung. Auch konnte die Ausbildung von fokal-konischen Domänen bei Schalen in der smektischen A-Phase für unterschiedliche Orientierungen an den Grenzschichten erklärt werden. Für Schalen, welche mit dem polymeren Tensid F127 stabilisiert wurden, konnte eine Änderung der Orientierung aufgrund der wechselnden Textur bei der Änderung der Temperatur beobachtet werden. Des Weiteren konnte erstmals der Phasenübergang von smektisch A zu smektisch C in Schalen mit homeotroper Orientierung beobachtet werden. Abschließend wurden flüssigkristalline Elastomerschalen mit nematischer Orientierung hergestellt. Durch das Aktuationsvermögen der Elastomer-Schale finden die Partikel Anwendung als Mikropumpen.

**Stichwörter:** Flüssigkristalle, Flüssigkristalline Elastomere, Nematische Schalen, Smektische Schalen, Kern-Schale Partikel, Mikropumpe, Doppemulsion



## This thesis is based on the following publications

- PAPER 1. [NEMATIC-SMECTIC TRANSITION UNDER CONFINEMENT IN LIQUID CRYSTALLINE COLLOIDAL SHELLS](#)  
Hsin-Ling Liang, Stefan Schymura, Per Rudquist and Jan Lagerwall  
*Phys. Rev. Lett.*, **106**, 247801 (2011)
- PAPER 2. [TOWARDS TUNABLE DEFECT ARRANGEMENTS IN SMECTIC LIQUID CRYSTAL SHELLS UTILIZING THE NEMATIC-SMECTIC TRANSITION IN HYBRID-ALIGNED GEOMETRIES](#)  
Hsin-Ling Liang, Rudolf Zentel, Per Rudquist and Jan Lagerwall  
*Soft Matter*, **8**, 5433 (2012)
- PAPER 3. [LIQUID CRYSTALS IN NOVEL GEOMETRIES PREPARED BY MICROFLUIDICS AND ELECTROSPINNING](#)  
Hsin-Ling Liang, Eva Enz, Guisy Scalia and Jan Lagerwall  
*Mol. Cryst. Liq. Cryst.*, **549**, 6977 (2011)
- PAPER 4. [TUNING THE DEFECT CONFIGURATIONS IN NEMATIC AND SMECTIC LIQUID CRYSTALLINE SHELLS](#)  
Hsin-Ling Liang, JungHyun Noh, Rudolf Zentel, Per Rudquist and Jan P. F. Lagerwall  
*Phil. Trans. R. Soc. A*, **371**, 20120258 (2013)
- PAPER 5. [TOWARDS MICROMETER SIZED CORE-SHELL ACTUATORS FROM LIQUID CRYSTALLINE ELASTOMERS BY A CONTINUOUS FLOW SYNTHESIS](#)  
Eva-Kirstina Fleischmann, Hsin-Ling Liang, Jan Lagerwall and Rudolf Zentel  
*Proc. of SPIE*, **8729**, 82790M-1 (2012)
- PAPER 6. [ONE-PIECE MICROPUMPS FROM LIQUID CRYSTALLINE CORE-SHELL PARTICLES](#)  
Eva-Kirstina Fleischmann, Hsin-Ling Liang, Nadia Kapernaum, Frank Giesselmann, Jan Lagerwall and Rudolf Zentel  
*Nat. Commun.*, DOI: 10.1038/ncomms2193 (2012)



# Contents

---

<b>Abstract</b>	<b>i</b>
<b>Zusammenfassung</b>	<b>iii</b>
<b>Publication included in the thesis</b>	<b>v</b>
<b>Table of contents</b>	<b>vii</b>
<b>1 Introduction</b>	<b>1</b>
1.1 Liquid crystals . . . . .	1
1.2 Liquid crystalline shells . . . . .	2
1.3 Goals and overview of this thesis work . . . . .	4
<b>2 Research background relevant for this work</b>	<b>6</b>
2.1 Structures of the most common phases of liquid crystals . . . . .	6
2.2 Liquid crystalline elastomers . . . . .	7
2.3 Polarizing microscopy and birefringence . . . . .	8
2.4 Director field deformations and topological defects . . . . .	10
2.4.1 Common defects and birefringent textures in the nematic phase . . . . .	11
2.4.2 Common defects and birefringent textures in the smectic phase . . . . .	13
2.5 Liquid crystals in spherical morphology . . . . .	14
2.6 Microfluidic production of multiple emulsions . . . . .	16
<b>3 Summary of results produced in this thesis work</b>	<b>19</b>
3.1 N to SmA transition under planar alignment . . . . .	20
3.2 N to SmA transition under hybrid alignment . . . . .	21
3.3 Topological transformation in relation to surface anchoring . . . . .	23
3.4 First observation of SmA to SmC transition under homeotropic alignment . . . . .	25
3.5 Liquid crystalline elastomer shells . . . . .	26
<b>4 Summary and outlook</b>	<b>27</b>
<b>References</b>	<b>28</b>
<b>Publications</b>	<b>31</b>
P 1. Nematic-smectic transition under confinement in liquid crystalline colloidal shells . . . . .	33
P 2. Towards tunable defect arrangements in smectic liquid crystal shells utilizing the nematic–smectic transition in hybrid-aligned geometries . . . . .	35
P 3. Liquid crystals in novel geometries prepared by microfluidics and electrospinning . . . . .	37
P 4. Tuning the defect configurations in nematic and smectic liquid crystalline shells . . . . .	39
P 5. Towards micrometer sized core-shell actuators from liquid crystalline elastomers by a continuous flow synthesis . . . . .	41
P 6. One-piece micropumps from liquid crystalline core-shell particles . . . . .	43
<b>Acknowledgements</b>	<b>45</b>



# 1 Introduction

Shapes of matter are play grounds of nature and of human manipulation, from mountains to snow crystals and from buildings to golden accessories. The human-designed shapes are engineered obeying natural laws and often introduced to business markets. The paradigm of liquid crystal studies in this pattern expands from flat film samples to the newer developments of fibers and/or colloidal composites, attracting scientists to the establishment of topological rules and the design of practical demonstrations. This thesis focuses on liquid crystals in the spherical shell geometry, one of several new branches that emerged in the recent decade. It deals with molecules ranging in size from a few benzene rings to macromolecular chains and networks, and it reveals intriguing phenomena, often related to reorganization of building blocks at phase transitions.

## 1.1 Liquid crystals

The concept of liquid crystals is founded on the classification of molecular order, which is summarized within the framework of the different *states of matter*. The states, or phases, describe how units of matter bond with respect to each other in space (the condensed phases) or distribute throughout the available volume without any kind of bonding (the gas phase). The phases commonly mentioned are solid, liquid and gas phases. Solids in a broader sense can be categorized into amorphous solids (glasses) and crystalline solids, where the latter possess a three-dimensional long-range positional order (2D crystal phases can arise in intrinsically two-dimensional systems such as colloidal crystal nucleation on a substrate or Langmuir monolayers). On the contrary, matter in the ordinary liquid and gas phases exhibits no long-range without order, and we may thus call them isotropic states (the word “isotropic” is derived from Greek: “iso”: equal; “tropos”: a turn, describing an object having equal physical properties in all directions). Liquid crystals possess, as the name suggests, a character between the liquid and the crystalline solid phases, exhibiting some intermediate degrees of molecular order. When an ordinary crystal is heated to the melting point, its lattice is destroyed and the substance transforms directly into the liquid state. There were however some solid substances found to form a transient turbid liquid at melting from the crystalline state before entering the liquid state. When the Austrian botanist Friedrich Reinitzer observed this phenomenon for the first time in 1888, in a cholesteryl benzoate sample, he was wise enough to not simply reject the unexpected behavior as an artifact caused by impurities. He described his sample as undergoing a *double melting* behavior.[1] This is regarded as the discovery of liquid crystals, where the second melting point is denoted today as the *clearing point*.

Back then Reinitzer investigated the turbid state of the matter with the German physicist Otto Lehmann, who used his skills with the polarizing microscope constructed with a heating stage, confirmed the existence of the intermediate phase and realized that the phase was optically anisotropic. The name *flowing crystals* was by then used to introduce this material class.[2] Their intermediate behavior was later declared as *mesomorphic states of matter* (or *mesophases*) by the French crystallographer George Friedel, and molecules that demonstrate mesophases are called *mesogens*. He also coined names to the different liquid crystal phases, *i.e.* nematic and smectic, which become the standard terms.[3] During the early twentieth century the German chemist Daniel Vorländer conducted systematic synthesis work and concluded that all compounds that present mesophases had elongated (rod-like, or calamitic) molecules. The structural concept of

mesogens was later enriched by reports on disk-like (discotic),[4] lath-like (or sanidic)[5] and the latest banana-shaped molecules,[6]. In summary, the fundamental requirement of liquid crystalline mesogens is the shape anisotropy (Fig. 1.1).

The shape of mesogens leads to anisotropic intermolecular interactions, which, in turn, induces a tendency of molecular packing along a certain direction. This gives the bulk sample long-range orientational (nematic) and sometimes also partially positional (smectic) ordering that lead to anisotropic properties like optical birefringence. Mesomorphic order has eventually been found to broadly exist in nature as a result of spontaneous ordered molecule aggregation in concentrated solutions of amphiphilic molecules, as well as in some polymers or their solutions, and in suspensions of shape-anisotropic particles. Systems whose liquid crystalline phases form only with solvents involved and mainly determined by concentration are classified as *lyotropic* liquid crystals, in contrast to *thermotropic* liquid crystals which are composed of pure compounds or homogenous mixtures and whose mesophase formation is temperature driven. This thesis is within the scheme of thermotropic liquid crystals, particularly with rod-like mesogens.

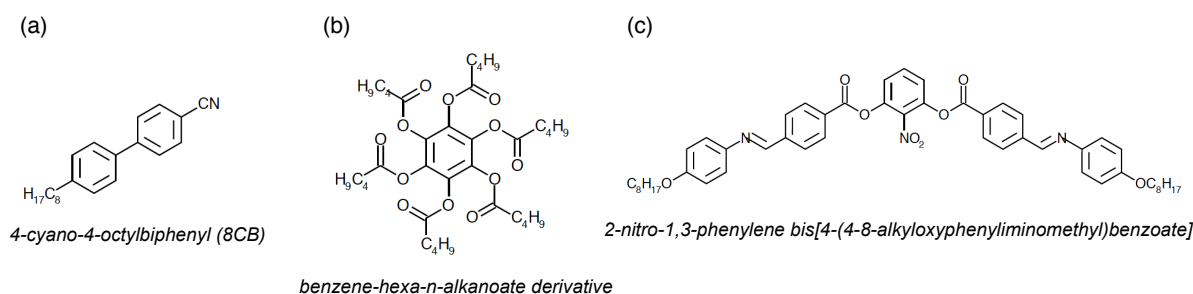


**Figure 1.1** Examples of molecular structures of liquid crystals for (a) calamitic, (b) discotic, and (c) banana shaped anisotropy.

## 1.2 Liquid crystalline shells

The discovery by Reinitzer and Lehmann of liquid crystalline character of the cholesteryl benzoate, originally derived from carrots, has its historical background in the fact that, in the middle of the nineteenth century biologists began to use polarizing microscopes for studying substances extracted from plants and animals. Back in the day liquid crystalline properties were revealed optically but the origin of the remarkable properties was not known. The early literature can be traced to the famous introduction to *myelin figures* in the 1850s,[7] which described the self-organization of myelin, a substance extracted from nerves that is rich in phospholipids, which in contact with water forms rolled-up cylinders. It was not until half a century later that the myelin forms were connected with the concept of liquid crystals,[8] and nowadays they are cited as the first documented lyotropic liquid crystals.

Phospholipids serve as the major content of cell membranes in almost all living organisms. In presence of water, phospholipids can arrange into bilayered and semipermeable closed sheets (Fig. 1.2a), so called *vesicles*, due to their amphiphilic nature. In 1985, certain vesicles were found to transform into open-ended helical ribbons or tubules below the temperature at which the aqueous phospholipid mixture goes through a phase transition from a high temperature mobile liquid crystalline phase to a low temperature gel-like state.[9] Upon heating the reverse process was observed. This phenomenon triggered

studies on the topology of vesicles—the *naturally occurring liquid crystalline shells*—with excitement about the possibility of the means of exploiting this in the creation of new self-assembled nanostructures as well as possible connections to certain diseases, for instance gallstones.

About half a decade later, Lubensky and Prost developed a model suggesting that the change of molecular orientation during the phase transition drove the vesicle deconstruction.[10] On cooling from the vesicle shape, phospholipids can transform from an arrangement without any in-plane ordering (the  $L_\alpha$  phase, the lyotropic analogue to what in thermotropic liquid crystals is called a smectic A (SmA) phase) to one where the symmetry within the membrane plane is broken by a uniform tilting of the molecules with respect to the membrane normal. This means that there is an added direction of long-range in-plane orientational order (the  $L_{\beta'}$  phase, analogue to the smectic C or higher ordered thermotropic smectic phases), see Fig. 1.2b. However, the in-plane directional profile cannot perfectly cover a spherical surface, since its topology requires the formation of defects with a consequent increase of elastic energy due to the distortion of the orientational field around each defect. This could force vesicles to break open in order to relieve the energy penalty (the topology of an open-ended tube requires no defects). This theory quantifies energy costs for defect structures of directional order (primarily represented by tangential nematic ordering, where the preferential orientation is described by the director field  $\mathbf{n}$ ) at a spherical surface, and on this basis Lubensky and Prost postulated that the ground state configuration of a spherical liquid crystal shell can consist of two unit singularities at two poles for a sign-sensitive orientational order ( $\mathbf{n} \neq -\mathbf{n}$ ) and four half-fold singularities located at the vertices of a tetrahedron for a sign-invariant orientational order ( $\mathbf{n} = -\mathbf{n}$ ) (Fig. 1.3).

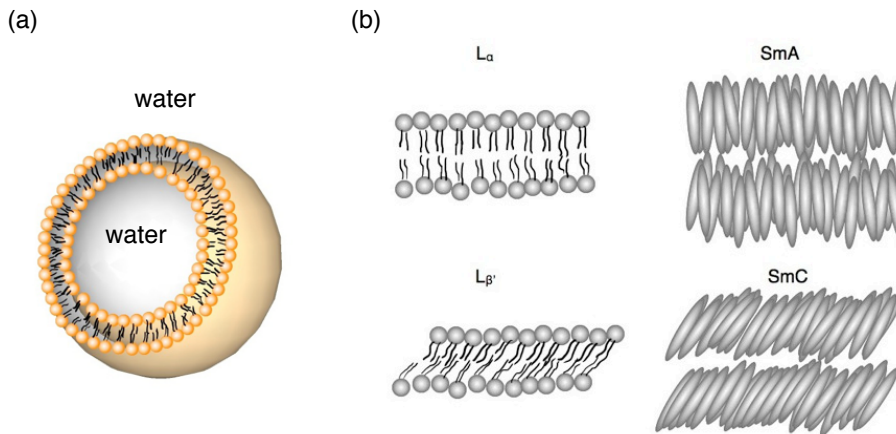


**Figure 1.2** Schematic representation of lamellar phases. (a) A vesicle, or more precisely for this case, liposome, in an aqueous environment consists of phospholipids arranging in a bilayer structure that forms a closed spherical shell (a cut through it has been made in the drawing in order to visualize the internal structure), with hydrophilic heads in contact with water. (b) Analogy between lamellar non-tilt  $L_\alpha$  and tilt  $L_{\beta'}$  phases with thermotropic SmA and SmC phases.

This prediction later on inspired a proposal by Nelson for an innovative strategy for advanced colloid crystallization, that relied on the functionalization of the defects using linkers.[11] This could turn the liquid crystalline shells into colloid particles with tetrahedrally directed interactions, allowing them to self-assemble into crystals with the same geometry as diamond, but with a colloidal scale lattice parameter. Such colloidal crystals

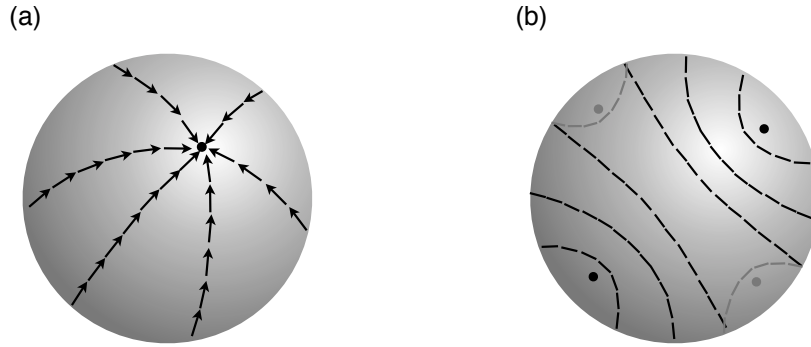


**Figure 1.3** Energetically preferential orientation on a spherical surface. (a) Two-fold defect configuration formed in the case of sign-sensitive orientational order. (b) Four-fold defect configuration organized into a tetrahedral structure in the case of sign-invariant orientational order (defects at the bottom hemisphere are shown in gray).

are of substantial interest for photonic applications. Five years later the theoretical predictions could for the first time be compared with experimental data, as Fernandez-Nieves and co-workers succeeded in fabricating nematic shells by a microfluidic method.[12] This offered direct observations of the predicted defect structures, but they exhibited asymmetric arrangements due to the non-negligible shell thickness. Since the free energy cost of a half-fold singularity (which is a defect line running through the shell, from the outer to the inner interface) is proportional to the shell thickness, the energy is minimized by gathering all four defects to the thinnest point of the shell. These groundbreaking articles inspired a lively new research field, with several interesting contributions following, pursuing both experimental and theoretical approaches.[13–17]

Studies on mesogenic order on curved surfaces are not limited to nematic ordering. As mentioned above the recent interest in liquid crystalline shells has a connection to the peculiar phenomena observed at transitions between lamellar phases in phospholipid vesicles, and the attempts to explain them revealed fundamental connections between lyotropic and thermotropic phases, primarily of lamellar/smectic types. Moreover, since the 80s smectic bubbles have been extensively investigated regarding their rupture dynamics owing to the similarity to soap bubbles[18, 19] (they are also in an  $L_\alpha$  phase); indeed, the term “smectic” originates from “soap” in Greek. In recent years, motivated by biological systems, smectic vesicles obtained by the self-assembly of tailor-designed amphiphilic block copolymers containing liquid crystalline side chains provided direct images of smectic order in spherical membranes,[20, 21] which were followed by theoretical models established for smectic ordering in the topology of closed surfaces.[22, 23] Very recently, attention was paid to shells of different variations of liquid crystalline materials. It was for instance demonstrated that cholesteric[24] and elastomeric[25] liquid crystals in shell geometry have potential for application as microlasers and micropumps, respectively. These cases set examples of the expansion of *thermotropic* liquid crystalline shells as smart tools for next generation self-assembled dynamic devices.

### 1.3 Goals and overview of this thesis work

While phospholipids can spontaneously aggregate into vesicle shape in water, thermotropic liquid crystals, in general immiscible with water, require the use of a special emulsification process to be stabilized in shells in aqueous environment, leading to a water-in-

oil-in-water (W/O/W) emulsion (where the liquid crystal plays the role of the oil phase). Surface tension ensures that spherical shape is the stable morphology, as seen in drops, or bubbles. The challenge lies in the reduction of the size distribution and the possibility to control shell thickness and diameter reliably. One of the most successful methods to produce monodisperse emulsions is the *microfluidic* technique, or more precisely *droplet microfluidics*,<sup>[26]</sup> which allows rapid fabrication of single and multiple emulsions.<sup>[27, 28]</sup> Microfluidics research is frequently done using channels embossed in soft chips made of polydimethylsiloxane (PDMS) elastomer. Alternatively the Weitz group at Harvard<sup>[29]</sup> presented a device built up by nested glass capillaries, with advantages of relatively high temperature and solvent resistance and of its simpler preparation process, which has become a prominent tool used to deliver particles of various materials down to the micro scale, including the first reported nematic shells.

This thesis work deals with deploying the glass capillary microfluidic set-up to obtain a wider arrangement of nematic and smectic shells. Liquid crystals, in particular those having more than one mesomorphic phase, frequently have relatively high clearing point, and they can be rather viscous or even crystallized at room temperature, rendering the control over their flow by the microfluidic method difficult. Therefore, the first stage of the work deals with fine modifications of the glass capillary microfluidic system, mainly the addition of heating controls for each component, allowing for a system capable of producing liquid crystalline shells at elevated temperature. This new set-up allows the main goal of the investigations of internal structural rearrangements of shells upon phase transitions under in-plane, out-of-plane, or mixed surface alignment. The last part is devoted to the production and the study of shells of elastomeric liquid crystals. Adapted from a prior design from our group for microfluidic synthesis,<sup>[30]</sup> the temperature-regulated glass capillary system is optimized for the fabrication of liquid crystalline core-shell elastomers via photo-polymerization during flow. This leads to the creation of actuating shells functioning as micropumps.

---

## 2 Research background relevant for this work

This section summarizes relevant issues concerned in this thesis. I will concisely introduce the structures of the most common liquid crystal phases, the polarization optics of the nematic phase in different geometries, topological defects and disclinations in nematic and smectic-A phases, before continuing with a review of precedent works on spherical liquid crystal samples. I end with an introduction to the experimental and investigation methods. The term “liquid crystals” mentioned in the following particularly stands for rod-like thermotropic liquid crystals, if not noted otherwise.

### 2.1 Structures of the most common phases of liquid crystals

The chemical structure of rod-like mesogens is in general composed of a rigid linearly extended core formed by *e.g.* phenyl groups, the two ends of which have flexible aliphatic chains attached. The shape of liquid crystals dominates their ordering and associates with their optical property. As in the crystal family, liquid crystals can be classified into a uniaxial or biaxial system according to the number of optic axes in the ordering. Uniaxiality is often portrayed by a rotationally symmetric ellipsoid. Looking along its main axis of symmetry the cross section would be circular and you could not distinguish the ellipsoid from a sphere (Fig. 2.1). Along this viewing direction the material thus appears isotropic, and this defines this direction as the optic axis. Nematic and SmA phases are normally uniaxial with the director indicating the optic axis. In a SmC phase, on the other hand, the molecular tilt in a layered structure biases the molecular rotations, breaking the rotational symmetry around the director field. One must therefore look in one of two symmetrically oriented directions away from the director in this biaxial phase, for the cross section to appear like a circle.

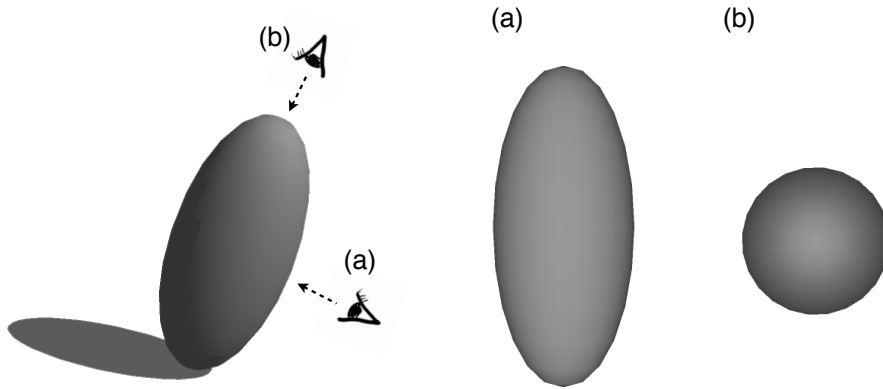


**Figure 2.1** A birefringent phase represented by a prolate ellipsoid possesses the optic axis along the geometrical long axis. Depending on the viewing direction it can appear as optically anisotropic (a) or isotropic (b).

Liquid crystalline phases are categorized according to the degrees of molecular order (Fig. 2.2). The phase without long-range order as in any ordinary liquid is called the isotropic phase (Iso). The nematic phase (N) is the intermediate phase of the highest temperature with the least order exhibiting solely orientational order along a preferential direction (the director  $\mathbf{n}$ ). For a uniaxial system the orientational order can be quantified by the *order parameter*  $S = \langle 3 \cos^2 \theta - 1 \rangle / 2$ , an average term that concerns the polar

angle  $\theta$  of the long axis of each molecule fluctuating in space with respect to  $\mathbf{n}$ . The typical value of  $S$  at room temperature is between 0.5 and 0.6 for nematics. With further decrease in temperature the nematic is often followed by the smectic phases (Sm), which show not only orientational order but also positional order. The positional order can be at the least one dimensional, leading to a layered structure of molecules' center of mass in the SmA and SmC phases. The SmA and SmC phases differ in whether molecules tilt with respect to the smectic layer normal  $\mathbf{k}$ . Three other relatively common smectic phases are SmB, SmI and SmF, with stronger positional order, but they are not discussed in this thesis.

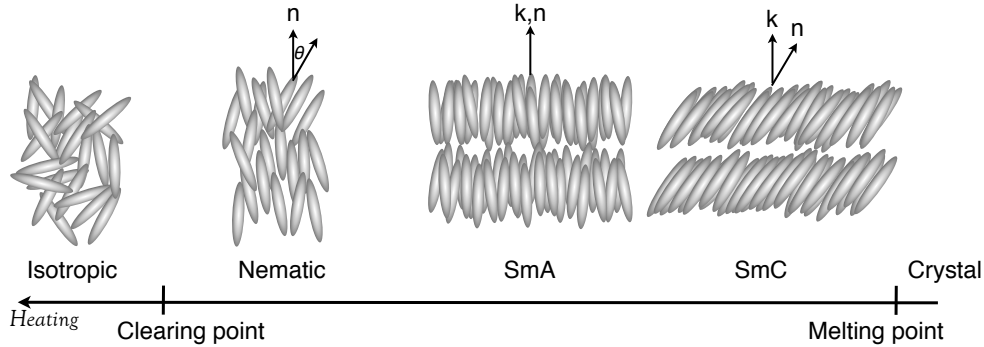


**Figure 2.2** Sketches of common thermotropic liquid crystalline phases. In the nematic phase,  $\theta$  represents the polar angle by which a single mesogen fluctuates in an instant with respect to the director  $\mathbf{n}$ . In smectic phases  $\mathbf{k}$  denotes the smectic layer normal.

## 2.2 Liquid crystalline elastomers

Elastomers are rubbery materials of slightly cross-linked polymer networks. When liquid crystalline mesogens are incorporated into polymer networks, the two species can affect each other's behavior. In highly cross-linked polymer networks, the preferential ordering of the mesogens can be preserved upon changes in temperature; while in lightly cross-linked polymer networks, the mesogens have certain mobility to reorient at phase transitions but the fluidity is resisted by the cross-linked networks.

The combination of liquid crystal mesogens and polymer networks was proposed by P-G. de Gennes and was anticipated for the uses as artificial muscles.[31] According to the attaching site of mesogens to the polymer backbone, three architectures of this combination can be classified, namely the main-chain, side-on and end-on side-chain polymers (Fig. 2.3a). The stiff liquid crystalline moieties in a lightly cross-linked liquid crystalline elastomer act as an anisotropic solvent, which imposes conformational anisotropy for the polymer chains. Upon the phase transition to the isotropic state of the mesogens, the polymer backbone regains the freedom to revert back to the spherical random coil conformation (Fig. 2.3b). The conformational change of the polymer backbone renders a shape change of the bulk liquid crystalline elastomer as an actuator, provided that the mesogenic orientation is uniform throughout the sample bulk in the liquid crystalline state. The preferential orientation can be obtained via mechanical stretching, electric and magnetic fields, lithography modelling, or flow stress. Over the last decades, different morphologies of liquid crystalline elastomers have been extensively fabricated, such as films, pillars, bars, particles...*etc.* Furthermore, the phase transition can be designed to

be external field- or light-driven, in addition to being induced by a temperature change, yielding various type of stimuli-responsive actuators.[32]

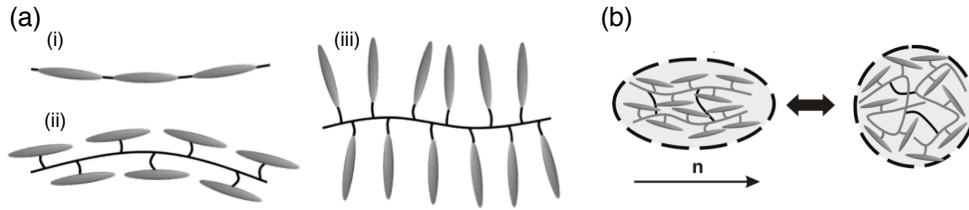


**Figure 2.3** Sketch of liquid crystalline elastomers (adapted from Ref. [32]). (a) The elastomers can be designed as stiff mesogens attached to the polymer backbone as (a) main-chain polymers (i), side-on side-chain polymers (ii) and end-on side-chain polymers. (b) The conformational change of the polymer backbone between the anisotropic (left) to the isotropic random coil (right) distribution, results from the loss and the recovery, respectively, of the orientational order upon the nematic–isotropic transition

## 2.3 Polarizing microscopy and birefringence

Polarizing microscopy is especially used in studies of birefringent materials, having the property of double refraction, earliest found in optical calcite in 1669, few decades after the establishment of the principle of refraction know as the Law of Snell. The use of polarized light has been a powerful tool to investigate the internal structure of crystals in crystallography at least for two centuries. Otto Lehmann, with his expertise on crystallography, is regarded to have been one of the first scientists to use polarizers in a microscope. A modern polarizing microscope is equipped with several additional components compared to a normal bright field microscope, named in the order along the light path: a polarizer filter, replacement of the fixed sample stage with a rotatable stage, a slot for insertion of wave plates, a second polarizer (also called *analyser*) that is usually rotatable and removable, and a Bertrand lens in some cases.

Light considered as a wave is a transverse wave with an electric field component that oscillates perpendicularly to its course of travel. *Unpolarized* light, as the sunlight, changes its direction of oscillation randomly, that is the polarization is undefined. A polarizer lets through only the portion of the light for which the electric field oscillates in a certain direction, and blocks the rest; therefore, it enables an extraction of light regarded useful for a purpose, as in the case of polarizing microscopy in which linear polarized light is usually used. When illuminating a sample placed in between of two linear polarizers, which are turned  $90^\circ$  with respect to each other's transmission directions (so-called *crossed polarizers*), all incoming light will be filtered out by the second polarizer, unless the sample is able to change the polarization of the light. Birefringent materials can thereby, due to their ability to do just this, be singled out in a polarizing microscope.

The refractive index ( $n$ ) of a medium represents the factor by which light slows down when entering the medium, as compared to the speed in vacuum, therefore a birefringent sample can split incoming light into two waves of different velocities (Fig. 2.4): the *ordinary* wave (o-wave) in which the electric field oscillates perpendicular to the optic axis experiences the refractive index  $n_o$ , and the *extraordinary* wave (e-wave) that oscillates parallel to the optic axis experiences the refractive index  $n_e$ . If the optic axis is not in the plane perpendicular to the propagation direction of the incoming light, the e-wave experiences the projection of the optic axis and thus a reduced  $n_e$  (assuming positive

optical anisotropy, *i.e.*  $n_e > n_o$ ). At the exit point e-wave and o-wave recombine with a phase shift given by  $\Delta\phi = \frac{2\pi}{\lambda}(n_e - n_o)h$ , where  $\lambda$  is the vacuum wavelength of the incoming light,  $h$  is the sample thickness and  $n_e - n_o = \Delta n$  is the effective birefringence of the sample (possibly with reduced  $n_e$  in case of an inclined optic axis, as mentioned above). If  $\Delta\phi$  has any value that is not an integer times  $2\pi$ , the recombined light change its polarization relative to the initial state.

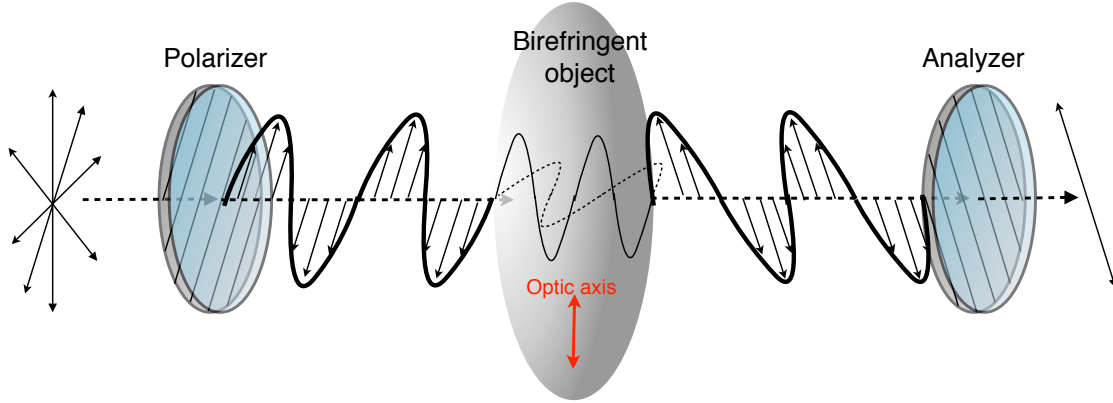


**Figure 2.4** Sketch of the light path in the presence of a birefringent object between crossed polarizers. The dashed arrows indicate the travel direction of light, while the thin arrows show the polarization direction. In the birefringent object the light splits into e-wave (solid line) and o-wave (dashed line). In this figure the phase shift between the o- and e-wave is graphed  $\lambda/2$ .

In other words, in the observation of birefringent materials between crossed polarizers the dark state (or the extinction) appears when the two waves travel in phase, namely  $\Delta\phi = 0$  or  $m2\pi$ ,  $m$  being an integer. The first case occurs when (1) the oscillating direction of the incoming light is either perpendicular or parallel to the (projection of) optic axis, hence sensing only  $n_e$  or  $n_o$ , but not both, or (2) the incoming light propagates along the optic axis, hence sensing an axially symmetric object (pseudo-isotropic or *homeotropic* status); in both situations there is no effective contribution from  $\Delta n$ . The second case occurs when o- and e-wave are phase shifted with respect to each other by full periods of  $\lambda$  in the medium, *i.e.*  $h\Delta n = m\lambda$ . For instance, when the sample with known  $\Delta n = 0.5$  is illuminated by linear polarized green light ( $\lambda \approx 500$  nm), the light can be blocked if the sample thickness happens to be 1, 2, 3  $\mu\text{m}$ ..., etc. In the other way around, when the sample thickness is known, possible values of  $\Delta n$  can be deduced. However, in practice the light source is normally white light, so what passes through the sample is perceived by eyes as a mixture of all colors, *e.g.* the blockage of green light with the exit of red and blue light results in the combination of a purple color. The interference depends on  $\Delta n$  and the sample thickness, and the effect is summarized in a *Michel Lévy Chart*, with the horizontal and vertical axis corresponding to the phase shift (in unit nm) and sample thickness (in unit  $\mu\text{m}$ ), respectively (Fig. 2.5a). In fact, a commercial optical compensator, so-called *wave plate*, is a birefringent material designed to create a specific phase shift for green light. A  $\lambda/4$  wave plate, for example, gives an added or subtracted  $\lambda/4 \approx 125$  nm phase shift (the plate is optimized for a wavelength of 500 nm) to a specimen depending on whether the optic axis of the specimen is parallel or perpendicular to that of the wave plate. The additional phase shift causes a color shift according to the Michel-Lévy Chart (Fig. 2.5b). It is therefore important to know the direction of the optic axis of a wave plate before the observation.

On the whole, the interaction between the oscillation of incoming light and the optic axis of a birefringent object forms the working principle of polarizing microscopy. The use of polarizers in a microscope defines the polarization of the incoming light and can accentuate birefringent colors of the sample while blocking the background light by crossed polarizers. Moreover, the determination of the direction of the optic axis is achievable in a polarizing microscope, by means such as rotating the sample (thus equipping the microscope with a rotatable stage) and inserting a wave plate. This possibility plays a crucial role in mapping the liquid crystal organization because the direction of the optic axis correlates to the director field  $\mathbf{n}$  (Fig. 2.5b).

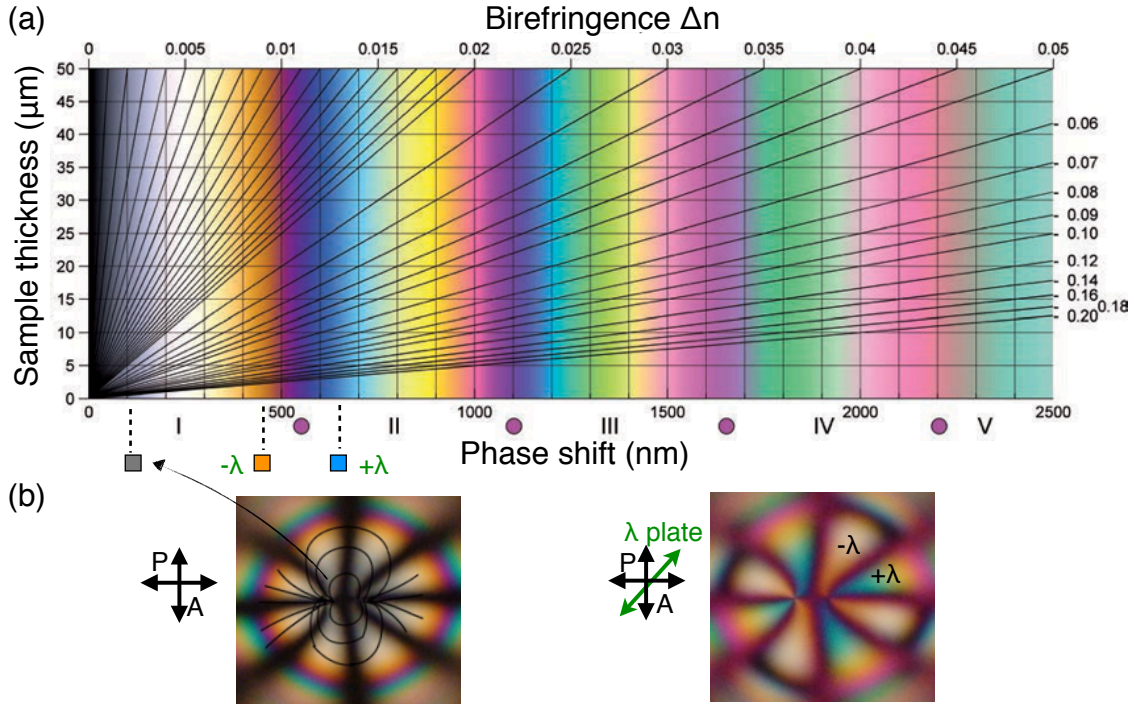


**Figure 2.5** (a) A recalculated Michel Lévy Chart, adapted from Sørensen, Eur. J. Mineral, 25, 5-10, 2013. (b) Example of using a  $\lambda$  wave plate with the aid of Michel Lévy Chart for the identification of the assumed director field (solid lines). The gray color at the regions near the center of the pattern shifts to blue or orange as a sign of addition or subtraction of a  $\lambda$  phase shift depending on whether the director field is parallel or perpendicular to the the optic axis of the  $\lambda$  plate. Note that the subtraction case changes the sign of birefringence, hence the “ $-\lambda$ ” case (orange box below the x axis) should be understood as being a mirrored Michel-Lévy diagram extending to the left of the origin of the actual diagram

## 2.4 Director field deformations and topological defects

The tendency of forming orientational order makes deformations of the director field cost energy. As liquid crystals possess smaller elastic constants than solids, the deformations occur rather easily in response to external influences, such as surface anchoring, confined geometries and external fields. Inspired by Otto Lehmann’s reports on “drop-forming liquid crystals”, what would be now called nucleating droplets driven by surface tension, the Swedish physicist Carl William Oseen was to figure out how the internal structure of liquid crystals fulfilled the confined geometry. He proposed several modes of director

deformations in his early work, the theory of which was further established by the Englishman Frederick Charles Frank and which become the known *Oseen-Frank formula*, describing the overall free energy density of nematic distortions:

$$F = \frac{1}{2}[K_1(\nabla \cdot \mathbf{n})^2 + K_2(\mathbf{n} \cdot \nabla \times \mathbf{n})^2 + K_3(\mathbf{n} \times \nabla \times \mathbf{n})^2]$$

where  $K_1$ ,  $K_2$  and  $K_3$  represent the three elementary elastic constants of *splay*, *twist*, and *bend* deformations. The generation of these deformations dominated by boundary conditions is shown in Figure. 2.6.

In practice, the creation of surface conditions is usually achieved by preparing liquid crystals on substrates treated with anchoring agents, *e.g.* polymers or surfactants, to induce planar or homeotropic (perpendicular) alignment, respectively (Fig. 2.7). The anchoring strength can be interpreted by how easily the molecules at the surface change their orientation. Under weak anchoring strength, topological defects are inevitably formed at where domains of different director meet.

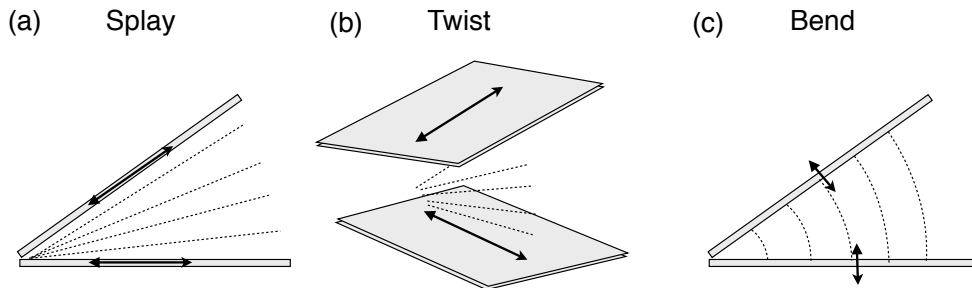


**Figure 2.6** Three basic modes of elastic deformation in a nematic fluid. The arrows indicate the molecular orientation at the boundaries.

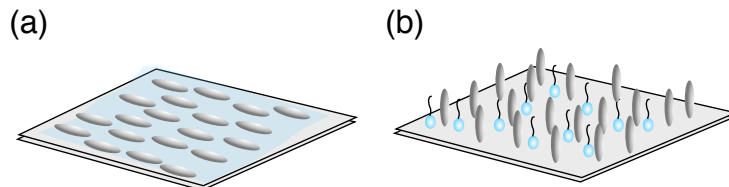


**Figure 2.7** Common surface anchoring treatment. (a) Planar alignment of liquid crystals can be obtained at a surface rubbed with polymers (polyimide, polyvinylalcohol (PVA), etc.) (b) Homeotropic alignment can be induced by a surface coated with surfactants.

#### 2.4.1 Common defects and birefringent textures in the nematic phase

Certain distortions create a molecular organization that is topologically incompatible with a continuous director field, rendering the formation of defects. Defects in liquid crystals are optically visible. In nematics there are two types of topological defects: defect lines and defect points. A defect line cannot end in the interior of a sample but either forms a closed loop or it has two termini attached to the sample surface(s) or to another defect.[33] If a defect line passes through the sample bulk aslant, its optical appearance is viewed as a thread, from which the phase “nematic” (thread in Greek) is named.

The way to define topological defect strength involves identifying the displacement

when taking a closed path around a defect. In crystals the displacement is dislocations of atoms, while in liquid crystals it encounters continuous inclination of the director field (in this sense Frank used the term “disinclination”, later shortened to *disclination*, referring to defect lines). Therefore, the defect strength ( $s$ ) in nematics can be represented by the number of turns that  $\mathbf{n}$  makes when winding along the loop:  $s = \frac{\Omega}{2\pi}$ , where  $\Omega$  is the angle by which the  $\mathbf{n}$  has turned.  $s$  can be positive or negative depending on whether the loop and the winding direction of  $\mathbf{n}$  are in the same sense or the opposite sense. Analogous to electric charges but due to elastic energy, the defects can repel or attract each other if they possess the same signs or opposite signs, respectively. They can merge into a new defect with strength equal to the sum of the strengths of the two original defects. In the case where two defects have the same magnitude but different signs, they can annihilate. The top view of the director topology adjacent in the vicinity of disclinations is shown in Figure. 2.8(a-d), together with the corresponding defect strength. It can be proven that an  $s = \pm 1$  disclination line is energetically unstable and can be avoided by rotating the director in the vicinity of the defect into the third dimension. In consequence, the defect line escapes, leaving two defect points at the surfaces (Fig. 2.8e). As the director diverges from one and converges to the other, the two defects (sometimes called *boojums*) form a topological pair.

The vicinity of defects is where the director field changes significantly, it therefore presents more distinctive optical features than elsewhere in polarizing light. Besides threads, the most common optical texture in nematics is the *schlieren* texture, illustrated by dark brushes spreading out from defects. The brushes are depicted in Figure. 2.8(a-d); note that they appear where the director field is perpendicular or parallel to the polarizers. While defects with the same magnitude but different signs exhibit the same set of brushes, a way to distinguish them is by rotating the sample stage: defects with brushes rotating in the opposite sense are charged positive, while defects with brushes moving in the same sense are charged negative.

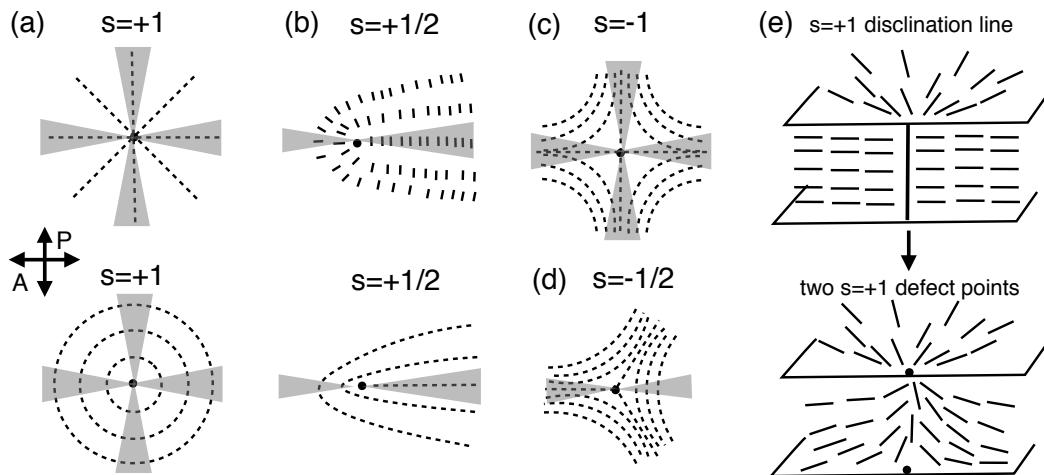


**Figure 2.8** (a-d) Top view of the director field in the vicinity of disclination cores. Shaded brushes indicate the region of the dark state which can be observed in the given crossed polarizers. (e) +1 disclination line melts into point defects by the relaxation of the director field (redrawn from Ref.[33]).

### 2.4.2 Common defects and birefringent textures in the smectic phase

In smectic phases molecules arrange themselves in equidistant layers. In this arrangement any change of layer thickness renders energetic penalty, hence this structure can adapt to the splay deformation by layer bending but is incompatible with the twist and bend deformation. The defects forming in the twist and bend deformations are often referred to the screw dislocations and the edge dislocations, respectively, which are related or can transform to the *focal conic* domains.[33] In the SmA phase *focal conics* are the most frequently occurring defects that were detected and named by G. Friedel. He observed that each domain is composed of an elliptic and a hyperbolic line (more precisely, a hyperbolic branch), by which he foresaw that they were focal lines of a group of curving parallel surfaces. The domains are formed by curved smectic layers in the geometry of Dupin cyclides. Given a proper proper boundary anchoring, they can transform into torus (which in fact is a special, fully symmetric, case of Dupin cyclide), where the defect hyperbola and ellipse degenerate into a straight line and a circle, respectively. (Fig. 2.9).

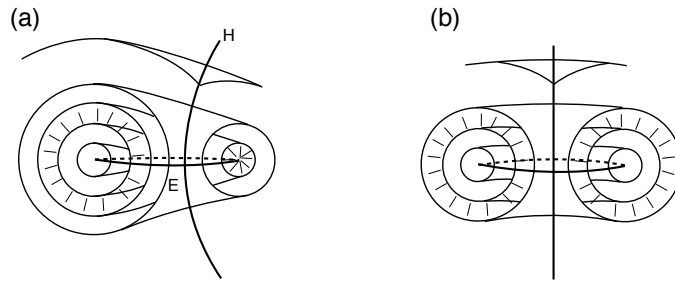


**Figure 2.9** Curved smectic layers in focal conic domains. (a) The ordinary domain in the form of Dupin cyclide yields a topological defect ellipse (E) and a defect hyperbola (H). (b) A toroidal domain, regarded as a special case of Dupin cyclide, has E and H degenerated into a defect circle and defect line, respectively. Redrawn from Ref. [34].

In thick preparations focal conic domains preferentially assemble into *polygonal textures*. In this geometry the whole sample volume is filled with several polygon domains, each of which contains iterative focal ellipses lying on one substrate surface with their coordinated hyperbolae passing through the sample bulk and joining at a vertex of another polygon at the opposite surface (Fig. 2.10 a,b). On the other hand, in thin preparations *fan-shaped textures* are often observed. The “slats” of the fans result from the sets of focal hyperbolae lying in the plane of the sample slide, and that the defect ellipses arrange perpendicular to the slide (Fig. 2.10 c,d). When the SmA focal conic domains are cooled to the SmC phase, due to the variation of molecular tilting direction, discontinuities of color often develop in the domains, resulting in the so-called *broken focal conic textures*.

Under perfect homeotropic condition, SmA samples appear dark between crossed polarizers as the viewing direction is along the optic axis. However, in the SmC phase the molecular tilt induces a directional field that exhibits schlieren texture similar to that in the nematic phase. The main difference lies in the absence of  $s = \pm\frac{1}{2}$  defects with the two-fold brushes in the SmC schlieren texture, as  $s = \pm\frac{1}{2}$  defects involve an azimuthal  $\pi$ -turn of the director field which is not allowed in the ordinary SmC directional field where  $\mathbf{n}$  and  $-\mathbf{n}$  are distinguishable.

Another common defect occurs in both homeotropic aligned SmA and SmC phase is the strings of small focal conic domains that result from smectic layer steps, typically observed in samples containing a thickness gradient, such as in a sessile drop on a substrate

treated to ensure homeotropic anchoring (Fig. 2.11). They are initially reported as the “terraced drop” by G. Friedel.

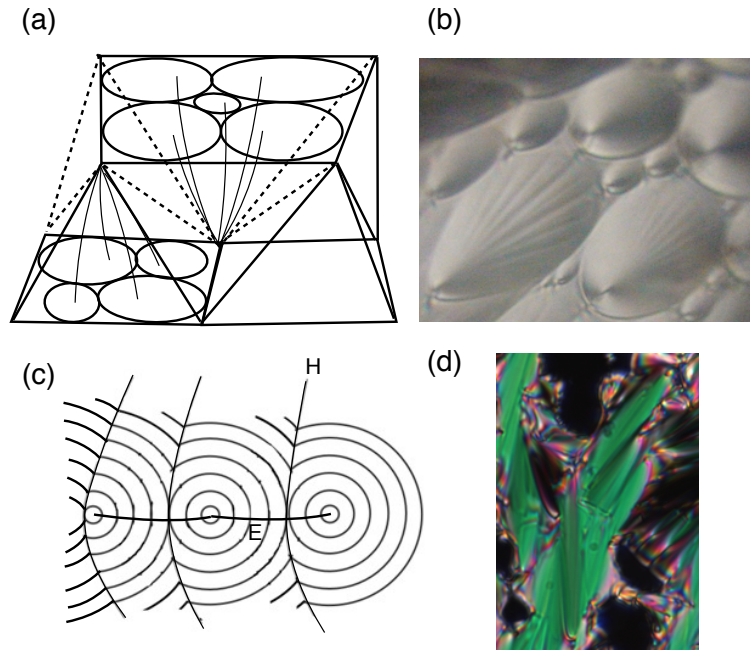


**Figure 2.10** Schematic structure (redrawn from Ref.[33]) of the polygonal texture (a), fan-shaped texture (c) and their correspondent direct images in polarizing microscopy (b,d). The polygonal and fan-shaped textures are distinguished by the defect features. In the former the ellipses, polygon edges and the projection of hyperbolae are visible, whereas in the latter the visible defects are the hyperbolae and the side projection of ellipses.

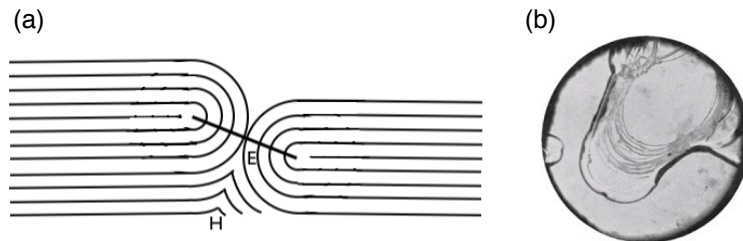


**Figure 2.11** (a) Schematic drawing of the structure of minuscule focal conic domains forming at smectic layer steps, of which a real image is shown in (b) from a seated smectic drop (adapted from Ref. [3]) on a substrate treated for homeotropic alignment.

## 2.5 Liquid crystals in spherical morphology

Spherical surfaces impose the requirement of deformations for liquid crystals to fulfill the geometrical condition, hence the introduction of topological defects is inevitable. In the nematic ordering the types of defects introduced in a sphere depend on the alignment of the liquid crystals. According to the topology rule,[35] for the tangential alignment the defect strength should sum up to  $s = +2$ , where the simplest arrangement is having two  $s = +1$  defect points separately located at the two poles (analogous to the singularities of time zones at the polar regions), where the repulsive distance is maximized. This defect

arrangement can form in the *bipolar* configuration, containing director splay and bend (the splay deformation is present near the defects, while the bend deformation is spread out along the meridian), or in the *concentric* configuration in the escaped mode, dictated by director bend (Fig. 2.12 a,b). Note that an ordinary concentric configuration endows an  $s = +1$  disclination line connecting the poles that can escape for lowering its energy, as previously mentioned. In the homeotropic alignment molecules should everywhere be perpendicular to the spherical surface, resulting in the *radial* configuration, where the director field converges at the core of the sphere and yields an  $s = +1$  singularity (so-called *hedgehog*) (Fig. 2.12 c). In the planar aligned SmA ordering, the spherical volume is filled with focal conic domains with hyperbolic branches no larger than the droplet radius (Fig. 2.12 d,e). Several studies have been conducted, considering the space filling of smectic layers in drops.[34, 36, 37]

The control of alignment plays an important role in the applications of droplet liquid crystals. The best known at the present day is the technique of polymer-dispersed-liquid-crystal (PDLC) system in uses such as privacy windows and display modules. The system contains approximately  $10^9$  liquid crystal droplets of  $1\ \mu\text{m}$  diameter embedded in a dried polymer matrix. It strongly scatters light at the initial state where each droplet possesses independent alignment, but can become transparent in response to an external electric field where the molecular orientation for all drops is in one direction. Recent advances of dispersed liquid crystals are presented as molecule detectors, especially explored in the biological field. If the absorbance of target molecules, such as viruses or proteins, is able to influence the alignment of liquid crystals, the change can be characterized optically by the defect configurations.[38–41] It is even found that the change of alignment can be due to the interaction between target molecules and the liquid crystalline defects rather than due to the absorbance effect.[42] The general advantage of dispersed liquid crystals is the lower requirement of the source material and the increase of sensitivity due to the larger surface-to-volume ratio compared to a bulk sample.

Besides the studies on applications, research on the process of alignment transformations has also been performed. It includes the bipolar–radial transformation by adding anchoring agents of the opposite type to the liquid crystal suspension thus changing the surface condition,[35] and the bipolar–concentric transformation induced by flow stress in the flat confinement of a microfluidic chip.[43] Later on with the experimental realization of liquid crystalline shells, nematic topological transformations induced by the change of anchoring condition is also studied in the shell morphology.[44, 45]

Spherical shells differ from drops by an additional inner surface. In the topology of planar nematic orientation at both surfaces, defects at the outer surface must have their counterparts at the inner surface. They are either disclination lines spanning through the shell bulk or pairs of boojums residing at both surfaces. There are three types of defect configurations often observed. Obeying the topological rule with  $s = +2$  defect sum at each spherical surface, they include four  $s = +\frac{1}{2}$  disclination lines (Fig. 2.13 a), one pair of  $s = +1$  boojums with two  $s = +\frac{1}{2}$  disclination lines (Fig. 2.13 b), and two pairs of  $s = +1$  boojums (Fig. 2.13 c).[12] Their geometrical arrangement is proposed to be varied with shell thickness and thickness inhomogeneity, which involves the competition between the collection of the defects at the thinnest point of the shell (driving the defects close to each other) and the repulsion between the same signed defects (driving the defects away from each other).[17] A successful fabrication of symmetric defect arrangements is achieved by thinning nematic shells via osmotic swelling, whereby the tetrahedral, isosceles triangle and linear defect geometries are obtained.[15] Although it is predicted that a  $s = +\frac{1}{2}$  de-

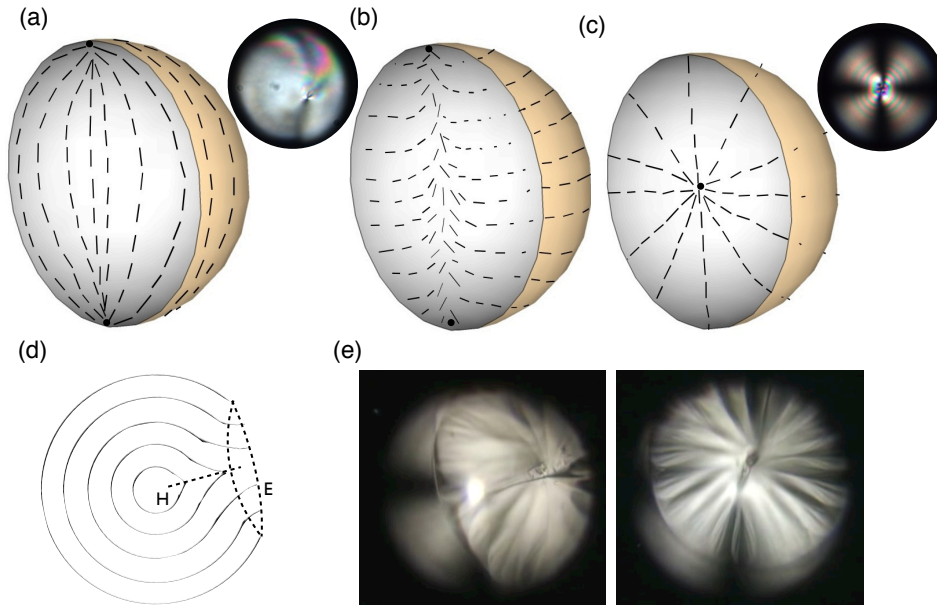


**Figure 2.12** Example of inner structures and optical images of nematic (a-c) and SmA (d,e) drops. Nematic planar alignment in spherical drops can be arranged in the bipolar (a) or (escaped) concentric (b) configuration with two  $+1$  point defects located at two poles. Homeotropic alignment is fulfilled by the radial configuration (c) with a sole point defect at the drop center. Inset photos are polarizing microscopy images correspondent to the bipolar and radial configuration. SmA drops in the planar dominance are typically of the space filling of polygonal domains. The simplest form filled by one focal conic domain (which can result from a degenerated planar anchoring condition) is depicted in (d) with direct images shown in (e). The defect hyperbola can be seen to span to the droplet center.

fect has lower energy than an  $s = +1$  defect does (by one-quarter for  $K_1 = K_3$ , by a half for  $K_1 \ll K_3$  [14]), splitting of an  $s = +1$  defect has not been experimentally detected. Shells under perfect homeotropic alignment are rather trivial to analyse. Compared to drops having a hedgehog defect in the core, the cavitory interior renders homeotropic shells defect-free (Fig. 2.13 d).

Liquid crystals in the spherical morphology can be produced by emulsification approaches, such as stirring, sonication or microfluidic techniques for example. The initial boundary alignment can be set by the anchoring agents dissolved in advance in the continuous phase. Microfluidic fabrication excels the other methods by the efficiency of reducing droplet size distribution and rapid production of multiple emulsion with controlled size. It has an important role in the modern research dealing with liquid crystalline shells.

## 2.6 Microfluidic production of multiple emulsions

Microfluidic systems deal with the transportation of nanoliter fluids, which, for example, exists in nature in the capillary network of a tree. Academic attention fell on microfluidic techniques during the era when the chemical weapons became new threats, where rapid and portable detectors were required.[46] They remain important in chemical and biological analyses, as the required volume of reagents decreases but the amount of data gained can significantly increase. A benevolent name “lab-on-a-chip” is given to the system of the sort. The applications extend to personal health diagnoses employed such as in spacecraft.

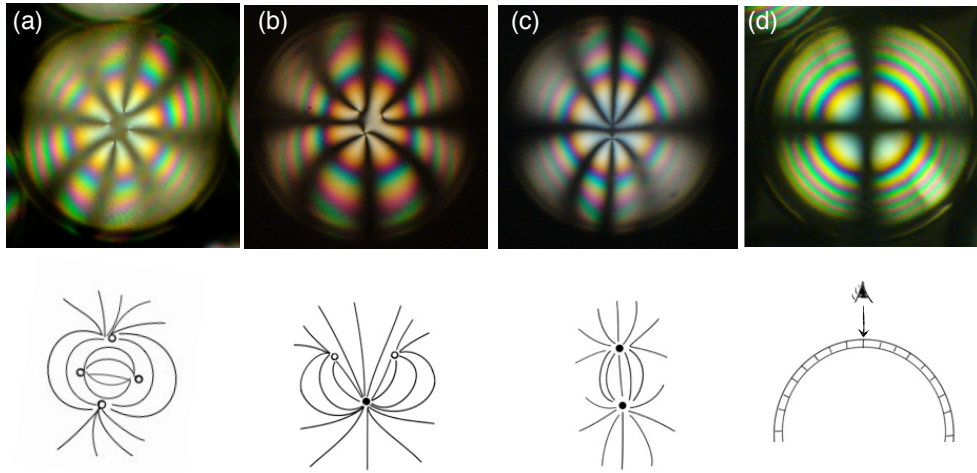


**Figure 2.13** Experimentally observed defect configurations in nematic shells (taken from shells discussed in Section 3.3). (a-c) Four-fold, three-fold and two-fold defect configurations. Their evaluated director fields are sketched at the bottom panel: the solid dots represent boojum defect points, whereas the hollow dots refer to  $s = +\frac{1}{2}$  disclination lines spanning the shell thickness. (d) The defect-free structure of shells under homeotropic alignment is characterized by interference rings and the “maltese” extinction cross. This texture results from the projection view that detects the gradually increased  $n_e$  (thus  $\Delta n$ ) of the shell towards the perimeter, leading to the birefringent color sequence in tune with the Michel Lévy Chart.

The base of microfluidics in the beginning was constructed by silicon or glass slides with etched channels made by photo-lithography. They became uncompetitive with the advent of polydimethylsiloxane (PDMS) chips invented by the Harvard professor G. Whitesides, who in recent years pioneered the development of paper-based analytical devices.[47]

The conventional production of capsular droplets (double-emulsion) is achieved by making the first emulsion, say W/O, via shear rupture, which is then drained at low speed into the second continuous phase, say water, resulting in the W/O/W emulsion. The process retains difficulties in control over size and encapsulation ratio. However, the drop formation in microfluidic devices is analogue to water drops dripping from a faucet, that the drop size is controlled by fluid flow rates. In the production of a double-emulsion, fluids of different phases (oil and water) flow in separate branch channels and are emulsified at the joining points. The emulsification process is continuous, thus called *one-step emulsification*. The production of multiple emulsion is then achieved by paralleling up the branch channels.[28]

For a while droplet microfluidic experiments were conducted in the above mentioned flat chips, where the drops moving in the channel are actually discotic. One-step microfluidic generation of intact spherical double emulsion was firstly demonstrated by Gánán-Calvo and Gordillo using a capillary flow focusing device, where he had demonstrated the size and thickness adjustability of the core-shell droplets by control of flow rates.[48] The method was improved with the invention of coaxial glass capillary microfluidic devices from the Weitz group at Harvard.[29] Numerous materials in the core-shell form have been produced in this kind of device, including, to name a few, polymersomes, liposomes, colloidosomes, core-shell hydrogels and liquid crystal shells.[27] The basic structure of the device is composed of two cylindrical capillaries in the scale of millimeter in diameter, the tips of which are narrowed into fine orifices of several micrometers. The tips are

then aligned opposite inside a capillary with square cross section (Fig. 2.14). The outer diameter of the cylindrical capillaries are in general chosen to fit the inner dimension of the square capillary to ensure the centering of the capillary alignment.

The production of a double emulsion involves three fluids: an inner fluid is injected into one of the cylindrical capillaries (injection tube), which is enwrapped at the orifice by a middle fluid flowing in the same direction through the voids between the injection tube and the square capillary. The co-flow formed by the inner and the middle fluids is then flow focused into the other cylindrical capillary (collection tube) by an outer fluid pumped in the direction opposite to that of the middle fluid. The flow focusing effect reduces the diameter of the co-flow, and thus promotes the Rayleigh-Pleateau instability driven by surface tension, resulting in the break-up of the co-flow into core-shell droplets in the collection tube.

Many creative devices can be made by extending the basic construction. Some accomplishments include a delicate repetition of co-flow segments, which has been demonstrated for producing multiple emulsions,[49] and the use of multibore glass capillaries to obtain multi-core shells.[50, 51] To achieve three dimensional flow is also a current aim for PDMS chips by design of stacked layers.[52, 53]

In the practical knowledge about the geometry of the co-flow and flow-focusing joint glass capillary device, the orifice diameter of the collection tube should not exceed three times that of the injection tube, and the distance between the two tips should be set comparable with the diameter of the collection tube. Moreover, due to the fact that the wetting of the injection tube with the inner fluid creates complexity of the co-flow formation, when necessary the injection tube should be surface modified to minimize the affinity of the inner fluid to the wall of the injection tube. For producing liquid crystalline shells liquid crystal materials are deployed as the middle fluid, and the chosen anchoring agents, which also act as emulsion stabilizers, are dissolved in the inner and the outer fluids (Fig. 2.14b).

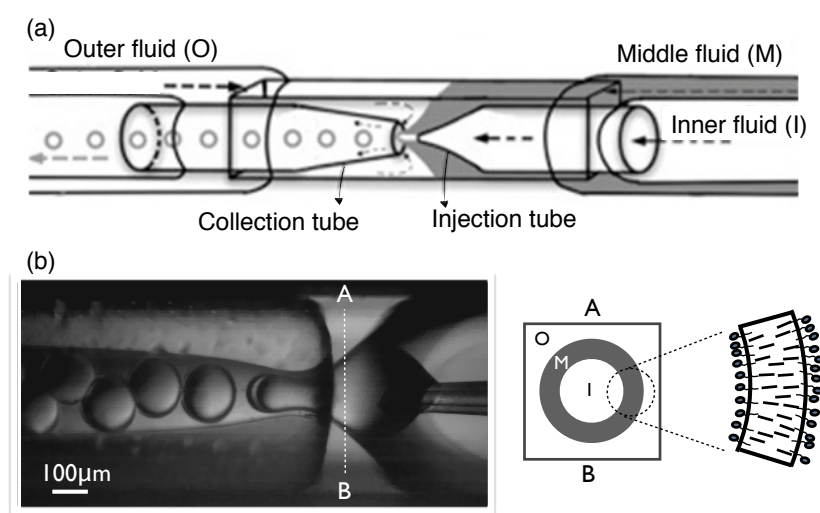


**Figure 2.14** Production of double-emulsion in glass capillary microfluidics. (a) Sketch of a co-flow and flow-focusing joint glass capillary microfluidic device. (b) Real image of the emulsification process captured by a high speed camera mounted on an optical microscope (left). Cross-sectional schematic A–B shows the production of homeotropic aligned liquid crystal shells. Surfactants, dissolved in the outer and the inner fluids, are used as emulsion stabilizers and anchoring agents (right).

### 3 Summary of results produced in this thesis work

Among the studies on liquid crystalline shells formed by low molar mass nematics, this thesis further concerns smectic ordering and liquid crystal elastomer shells with the aid of microfluidic methods. The methods allow for the fabrication of shells from different liquid crystal materials with different phases and variation of shell size and thickness.

The spherical geometry of liquid crystal shells results in a definite defect sum. On the theoretical ground, the equilibrium state of the defect configurations is predicted for mesogenic order on a two-dimensional sphere neglecting shell thickness. In reality, experimentally produced shells are as a three dimensional objects confined between spherical boundaries, and hence, due to the non-zero thickness and its spatial variations, the predicted state may not be achieved. Therefore, control of alignment, for instance by external influence, is crucial for the studies of liquid crystal shells towards the equilibrium state.

The new results of this thesis work can be organized into two topics. The first topic focuses on the fundamental investigation of topological configurations. This part deals with the influence of the geometry constraint and the surface alignment in shells on the development of defect structures in nematic, SmA and SmC ordering upon phase transitions. The alignment is enforced by the surface adsorption of anchoring agents. Similar to the surface treatment for flat preparations (Fig.2.7), the anchoring agents can be polymers or surfactants for the imposition of planar and homeotropic alignment, respectively. Since they also technically serve as shell stabilizers, the frustrating situation may arise that a good surface anchoring group is not necessarily a good stabilizer, and good stabilizers may yield peculiar effects on the liquid crystalline alignment.

In short, the results of this part are summarized in the following sections: Section 3.1 reveals the first optical analysis of shells upon nematic to SmA phase transition under planar alignment, where a unique buckling texture develops due to smectic layer undulation as undergoing the curvature strain of the shell geometry; Section 3.2 deals with the formation of rich focal conic domains in SmA shells under hybrid alignment; in Section 3.3 we discuss a peculiar alignment transformation from planar to homeotropic on heating in shells decorated by polymeric surfactants F127; Section 3.4 offers an initial observation on SmC shells under homeotropic alignment.

The second topic concerns the use of a controlled director field to achieve coordinated actuation in core-shell particles from liquid crystalline elastomers. The actuation behavior is in relation to the director field and requires overall preferential orientation. The strategy in this case for imposing uniform alignment is using the shear stress provided by the microfluidic flow. The reactive mesogens are aligned in the nematic phase and photo-polymerized downstream.

The result of this topic is shown in the Section 3.5, where uniformly oriented liquid crystalline elastomer shells are presented, and their actuating behavior is demonstrated. The shell actuators can be regarded as hart-like micropumps, capable of expelling the inner liquid out of the shell volume.

### 3.1 N to SmA transition under planar alignment

Shells of smectogenic liquid crystal 4-cyano-4-octylbiphenyl (8CB: SmA 33.5 N 41.5 Iso./°C) are ensured planar alignment at the boundaries (achievable by adding polymers, *e.g.* PVA, at the inner and outer aqueous phases). The tangential orientation is confirmed by the presence of the four-fold  $+\frac{1}{2}$  disclination in the nematic phase. Due to the thickness inhomogeneity induced by the density mismatch between the shell and the core, the disclinations gather at the site where the shell is thinnest. They however remain at a minimum distance from each other as a result of the director elastic repulsion. The defect structure is topologically identical to its symmetrical version of a tetrahedral arrangement (Fig. 1.3b), as the director field can be continuously deformed from one configuration to the other. When the defects are pulled together from the tetrahedral symmetry, they can be identified into two pairs, one of which is dominated by director splay and the other is governed by bend distortion. Given that the elastic constants of 8CB have been established  $K_3 \approx 2K_1$ , the director bend yields higher elastic energy density and this should drive its defect pair to the thinnest part of the shell than the director splay does (Fig. 3.1 a). On cooling to the smectic phase where  $K_3/K_1$  increases, the defects migrate apart from each other and would eventually lie on a great circle with  $\pi/2$  separation. This scenario is in agreement with theoretical predictions, that for a nematic spherical membrane the ground state defect configuration can transform from the tetrahedral to the great circle symmetry as  $K_1/K_3 \rightarrow \infty$ . [13, 14]

When the shell becomes smectic, the director bend within the cross section plane imposed by the shell curvature causes smectic layer dilation towards the outer surface. When the dilation is above a threshold value, the layers start to relieve the energy cost by undulation (Fig. 3.1 b). With our shells of curvature ratio around 0.95 between the outer and inner surfaces, a pattern caused by two generations of layer undulation is observed. The primary undulation occurs at the onset of nematic–SmA transition in order to resolve the stress induced by the surface curving direction parallel to the director field. This is perceived by the buckling stripes in the direction of the initial nematic director, which tile the shell with lune-shaped segments. In the adjacent lunes the layers tilt in the mirrored sense. The layer undulations in consequence rotate the director field which is now under the curvature stress of the perpendicular fraction, resulting in the second generation of the layer undulation within the lunes (Fig. 3.1 c).

According to the Helfrich-Hurault instability, if the undulation amplitude reaches the order of the layer thickness, layer edges may nucleate and even transform to focal conic domains under higher dilation stresses. [54] This is observed in thicker shells among our unpublished results.

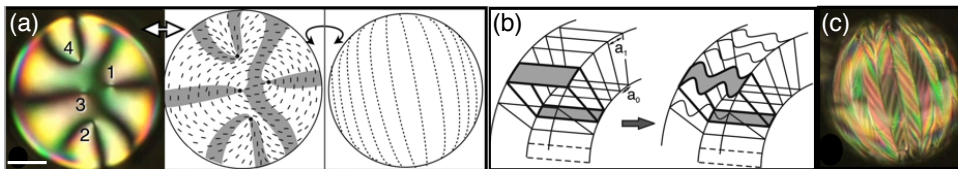


**Figure 3.1** Key features of 8CB shells under planar alignment. (a) The clustered four-fold defect configuration in the nematic phase can be distinguished between two pairs: defects 1 and 3 connect to director bend, while director splay dominates defect 2 and 4. (Scale bar=25  $\mu\text{m}$ ) The director field is drawn for the thin side of the shell where the defects are present (left) and the thick side (right). (b) Smectic layer dilation caused by the curvature strain is resolved by layer undulation, which results in the buckling texture shown in (c).

### 3.2 N to SmA transition under hybrid alignment

The *hybrid* alignment described here refers to shells having conflicting alignments at the two surfaces, namely planar alignment at one shell surface and homeotropic alignment at the other. The configuration renders a splay-bend deformation within the nematic shell bulk and causes layer bending in the smectic phase. In a thin preparation of a flat sample under hybrid anchoring, bent layers form an array of half cylinders,[55] whereas in a thick preparation periodic toroidal domains can be obtained (Fig. 3.2). Delicate fabrication of regular distributed toroidal defects deployed as lithography templates, arrayed microlens and particle trappers is finely demonstrated by Kim and co-workers.[56]

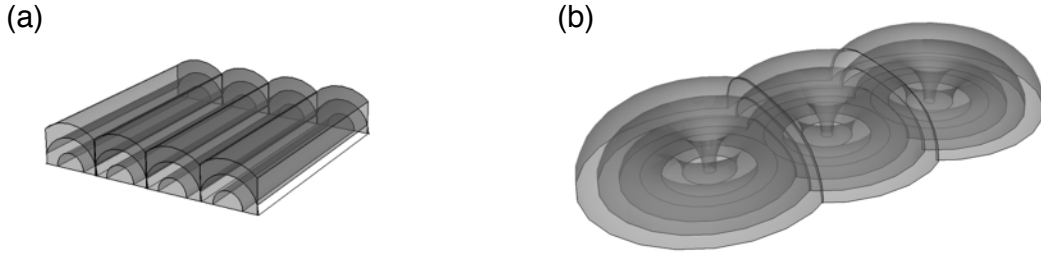


**Figure 3.2** Flat SmA samples with hybrid surface condition. (a) Arrays of cylindrical layers form in thin preparation. (b) Toroidal domains obtained in thick preparation.

In this topic we offer an investigation of the formation process of focal conic/toroidal defects as the shell undergoes the nematic to SmA transition in the shell geometry of 8CB. The director splay-bend provokes sign variance of the director field ( $\mathbf{n} \neq -\mathbf{n}$ ), therefore  $\mathbf{n}$  is treated as a sign-sensitive field, which renders the shells a two-fold defect structure in the nematic phase as shown in Figure. 1.3a. The two +1 defects can be considered as two separated boojums located at the two poles of the surface where the director field is planar oriented (Fig. 3.3 a,c). The planar director field is determined to be bipolar (instead of concentric) using a wave plate. At the onset of the transition to the SmA phase, smectic layers preferentially grow from the surfaces where the director is bending-free. However, due to the hybrid alignment the layer normals at the two regimes are perpendicular to each other. The antagonistic organization of layers at top and bottom is mediated by an increasingly compressed bend deformation in a thinning internal nematic membrane. According to Cladiz and Torza,[57] the nematic–SmA transition temperature is suppressed, allowing for this resolution of the frustration. The membrane tends to modulate out-of-plane in order to reduce the elastic energy, resulting in a striped pattern (Fig. 3.3 d). On further decrease in temperature, the shells eventually become fully smectic, where the director bend is solved by layer bending into focal conic (or toroidal) domains. The process is interpreted by the Rayleigh-Plateau instability. Upon cooling the surface tension between the nematic and the smectic regions can no longer sustain the striped smectic regimes, hence breaking them into focal conic domains (Fig. 3.3 e). In the hybrid shells we obtain nearly spherical focal conic domains. Since the domain radius cannot exceed the shell thickness, the size of the focal conic domains can be effectively tuned by adjusting the shell thickness. The transition features are shell size- and anchoring strength-dependent. In the cases of small shell size and/or strong homeotropic anchoring focal conic domains become unstable, and the shells instead transform to a full homeotropic arrangement in the smectic phase (sometimes leave minuscule focal conic domains at the smectic layer steps), despite the presence of planar anchoring agents.

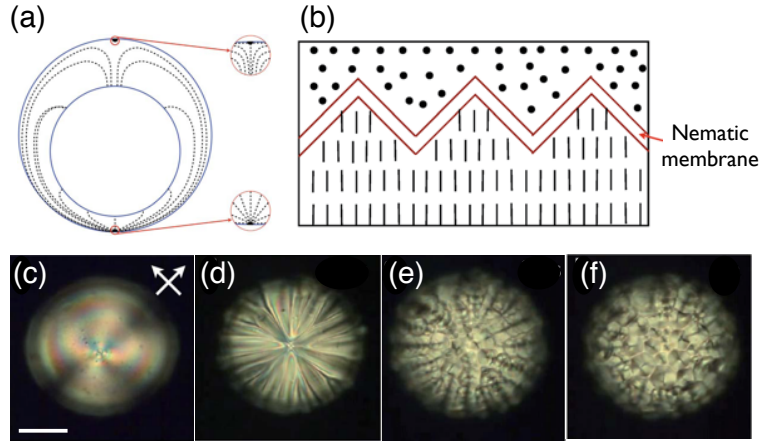


**Figure 3.3** Formation of focal conic domains upon nematic to  $SmA$  transition in an 8CB shell under hybrid alignment. (a) The director splay-bend in the shell bulk renders defect boojums at the two poles. The defect at the top of the shell is shown in (c). (b) On cooling to the  $SmA$  phase, a thin wrinkled membrane of nematic director bend is sandwiched by smectic layers, resulting in the striped pattern in (d). When the shell becomes smectic the stripes break up into focal conic domains due to the Rayleigh instability. (Scale bar= $50\ \mu\text{m}$ )

The stripes result from the peaks and valleys of the modulation plane extending along the direction of the director splay-bend. In consequence, the stripes can indicate the original planar director field. One shell that we studied by chance contained a dust particle, which seeded an additional defect besides the boojum pair. In order to still fulfill the condition that the defect sum is  $+2$ , the liquid crystal must form a  $-1$  defect next to the surplus  $+1$  defect seeded by the particle. This is confirmed by studying the striped texture that develops during the phase transition (double-confirmed by means of rotating the sample stage and observing the moving directions of the dark brushes), clearly revealing the presence of a positive-negative defect couple (Fig. 3.4). In order to remain the  $s = +2$  defect sum, other defects with total strength  $+1$  should be generated. The phenomena indicates that the use of alien particles is therefore a potential method for tuning defect configurations. In the meantime this was also demonstrated by Gharbi *et al.* in a recent article on nematic shells doped with particles.[58]

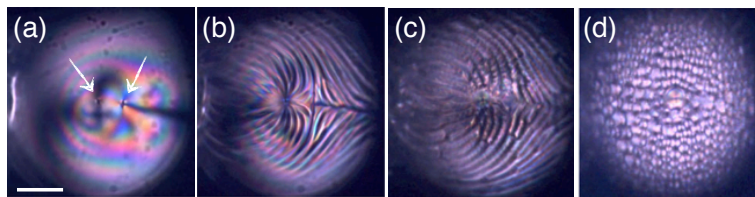


**Figure 3.4** The director of a shell containing a dust particle generates a defect with minus strength. (a-b) The texture of the director field is indicated by the striped pattern in the hybrid aligned shell, showing the defect at the left side is of strength  $+1$  and the one at the right is charged  $-1$ . (c-d) As the stripes break into focal conic domains, the  $-1$  defect becomes undetectable whereas the  $+1$  defect is fixed in position and form the largest focal conic domain. We thus assume that the  $+1$  defect is seeded by the dust particle. (Scale bar= $50\ \mu\text{m}$ )

### 3.3 Topological transformation in relation to surface anchoring

While searching for other possibilities of anchoring agents, we found intriguing alignment transformation phenomena induced by the polymeric surfactant F127 (PEO<sub>99</sub>-PPO<sub>67</sub>-PEO<sub>99</sub>). In the SmA phase of 8CB shells decorated with F127 at both surfaces, planar alignment is observed as evidenced by the buckling texture (Fig. 3.5 e). The alignment however transforms into homeotropic (Fig. 3.5 a) upon the transition to the nematic phase. The drastic change in texture involves a random handedness spiral pattern, possibly indicating a “domino effect” style of realignment process (Fig. 3.5 b-c). The previously reported molecular reorientation in shells[45] was induced by the change of anchoring agents, however in this case the reorientation occurs simply upon the temperature change. It is tempting to think that the effect is related to the lower critical micelle temperature (CMT) nature of F127, where PPO blocks dehydrate on heating, thus inducing homeotropic anchoring. However, according to the concentration of F127 in our system (5 wt%), the CMT would be around 23°C, which is quite below the nematic to SmA transition temperature of 8CB (33°C). In order to probe the phenomenon we further use the nematic mixture E7 (N 58 Iso.°C) as the shell material. We find that the planar alignment feature at the nematic phase gradually changes on heating from room temperature and eventually transforms into fully homeotropic alignment near the clearing point.

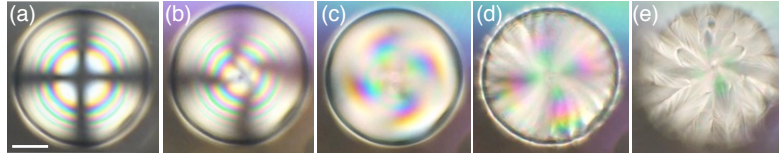


**Figure 3.5** (a-e) Nematic to SmA transition of an 8CB shell stabilized by F127. The reversed heating process is qualitatively the same in texture, involving the twist of the maltese cross that indicates the spiral form of the director reorientation. (Scale bar=50  $\mu\text{m}$ )

The results from E7 shells reveal another uncommon feature of the alignment, presumably a texture mixed by the planar and homeotropic alignment. Though the planar orientation is confirmed by the four-fold defect configuration, the rings of interference colors are in visible. The color rings typically appearing in the homeotropic alignment are never seen in our 8CB shells under fully planar alignment as ensured by PVA in both inner and outer phases. The surprising texture could be due to the larger birefringence of E7 (0.23) than that of 8CB (0.16), giving E7 a broader range of interference color than 8CB at the same sample thickness gradient; on the other hand, a degenerated anchoring effect of F127 can also be contemplated, where mesogens slightly tilt at the surfaces.

The “lemon”-shaped color rings can be explained by the details of the director field (Fig. 3.6 a). Again assuming a four-fold defect configuration where both director bend and splay are present, we can conclude that the loss of birefringence must be stronger in the region of director splay than in that of director bend. This is because molecules forming director splay at a curved surface is, for an observer, tilting away from the viewing direction, hence there is an apparent reduction in  $n_e$  (thus  $\Delta n$ ) towards the perimeter. In contrast, for director bend the long axis of molecules remains detectable in its full length despite the presence of curvature (Fig. 3.6 b), therefore more color rings can be observed in this region. The difference increases upon approaching the shell perimeter, explaining why the “lemon”-shape character gets stronger and stronger further away from the defects.

The first part of the reorientation scenario is similar to the result of Ref. [45]. First, two  $\pi$ -jump defect lines connecting the defect pairs are generated due to molecular tilts in opposite directions, as an initial step towards homeotropic anchoring (Fig. 3.6 c); second, the defect lines shrink in order to minimize the energy cost, resulting in the coalescence of defects (Fig. 3.6 d-h). During the process, the change in color indicates that the birefringence is substantially reduced, suggesting the tilt angle can be nearly perpendicular to the viewing direction; yet the persistence of defects indicates that a certain degree of tangential direction still remains. The last part of the realignment involves the previously mentioned “spiral” pattern, where the molecules begin to rotate in order to be perpendicular to the surfaces. At the final state the typical texture of birefringent rings in the defect-free homeotropic aligned shell is presented (Fig. 3.6 i-j). On cooling back, the spiral pattern reappears at the two poles forming a two-fold defect configuration similar to the realignment process in a droplet explained in Ref. [35]. The two defects remain as +1 defects without splitting back to the four-fold configuration (Fig. 3.6 k-o).

We can for now assume that the phase transition must play a secondary role in the reorientation of the director in the F127-stabilized 8CB shell. Possibly the sudden reduction of viscosity permitting the penetration of the PPO blocks into the liquid crystal plays a role. A concrete conclusion cannot be given without further investigations of the mechanism.

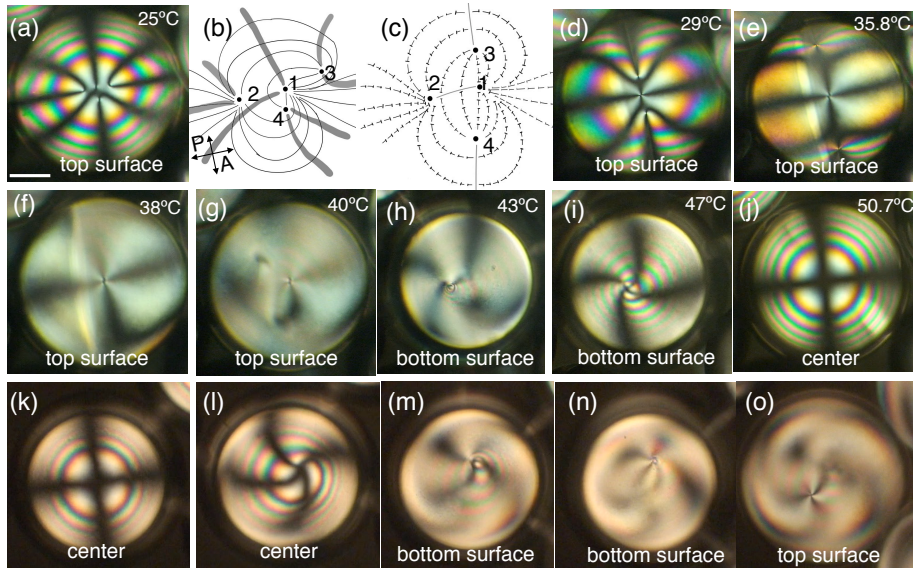


**Figure 3.6** Alignment transformation of E7 shells anchored by F127. The focal plane is noted in each optical image. (a) Shell with four-fold defect configuration in the nematic phase, where the deduced director field is drawn (slightly enlarged) in (b). The relative position of defects is evaluated from the real time movie, where the displacement of defect 3 is observed before the starting point of the realignment. On a curved surface the director bend and director splay yield a quantitative difference in birefringence, where the reduction of  $n_e$  is more significant in director splay. Therefore the birefringent rings have larger diameter and cover less color sequence at the region of director splay. (c-d) Two  $\pi$ -turn defect lines connecting defect pairs due to molecules tilting in opposite directions form at the onset of the reorientation process. (d-h) The shrinkage of defect lines causes the coalescence of the defect pairs, where the defect pair 2 and 4 traverses to the bottom hemisphere. (i-j) Suggested by the spiral pattern molecules that tilt along the planar director now rotate to fulfill the homeotropic condition. (k-o) The shell of homeotropic alignment reverses to tangential orientation on cooling via the spiral of molecular rotation, resulting in the 2-fold defect configuration as the steady state. (Scale bar=50  $\mu\text{m}$ )

### 3.4 First observation of SmA to SmC transition under homeotropic alignment

This Section is considered as a preliminary demonstration of the thermotropic counterparts of  $L_\alpha$  to  $L_{\beta'}$  transition in shell geometry. The chosen smectogens are a binary mixture of phenylpyrimidine: 2-(4-hexyloxyphenyl)-5-octylpyrimidine and 2-(4-octyloxyphenyl)-5-octylpyrimidine at 50/50 mass ratio (SmC 53 SmA 68 N 72 Iso./°C).

At room temperature the pure compound of each is crystallized, while the mixture is liquid crystalline, that reduces difficulties for the shell observation and stabilization. The homeotropic alignment is confirmed by the clear maltese cross (Fig. 3.7 a) in the SmA phase. Upon cooling the SmC phase is characterized by the melting of the cross and the nucleation of defects because the tangential order induced by molecular tilts (Fig. 3.7 b-e). The biaxiality of this phase presents rather complex distortion in texture, which makes it difficult to analyze the director field. In some cases it is not easy to spot the defects that ought to be present, which may be due that the defects are in fact not present: the LC could avoid the defects by locally reducing the tilt to zero, shifting the system to a SmA state at the point where the defect would have been.

Besides the above mentioned textual development, the complexity of the SmC director field renders several unexpected features. For example, in some shells a “grid” pattern tiling the surface (Fig. 3.7 f) is observed, which is very much like the lattice of parabolic focal conic domains,[56] but the actual details remain unclear. The studies of SmA–SmC transition is still in an infant stage though, we have shown the possibility of the production of SmC shells, allowing for deeper investigations.

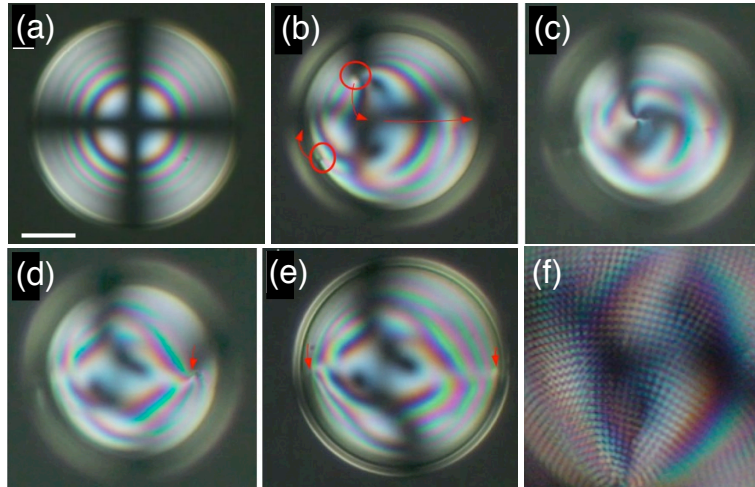


**Figure 3.7** (a-e) SmA to SmC transition under homeotropic alignment. The tangential alignment induced by SmC molecular tilts creates local defects (red circles). The arrows indicate the movement of the regions on cooling. In this case they exhibit a repellant behavior. (f) The lattice pattern with the similarity to parabolic focal conic domains found on the outer surface of some SmC shells. The magnification is twice larger than that of (a-c). (Scale bar=50  $\mu\text{m}$ )

### 3.5 Liquid crystalline elastomer shells

In this Section we demonstrate the fabrication of core-shell microactuators from liquid crystal elastomers. The device we build up here is of the co-flow geometry with two nested glass capillaries confined in a teflon tubing (Fig. 3.8 a). The device is retained in a heating block for the shell production. The outflow tubing is connected to an external hot stage for the photopolymerization process. In the microfluidic fabrication, the shell material is a mixture containing nematogenic monomers, photo-initiator and crosslinkers, the core fluid is glycerol, and the outer fluid is silicone oil. The whole shell formation process is kept at  $90^{\circ}\text{C}$  above the clearing point of the monomers ( $80^{\circ}$ ) for the sake of fluidity, and then the monomer shells are cooled to the nematic state ( $60^{\circ}\text{C}$ ) on the external hot stage. During the continuous flow of the nematic monomer shells, the orientation is also configured by the flow shear force exerted by the silicon oil. At a certain distance downstream the monomers are polymerized into core-shell elastomers. An advantage we take from the co-flow method is a compensation for the absence of emulsion stabilizers introduced in this shell production. In the co-flow geometry, the speed of the shell production can be slowed down, because the capillary bridging between the capillary orifice and the shell fluid can delay the detachment of monomer shells, which prevents the collision of shells before the polymerization process.

The orientation of core-shell elastomers is established by X-ray measurements, which confirm the shells possessing the bipolar configuration. This is assumed to be the result from the internal flow of the shell and the glycerol core (Fig. 3.8 b). The shape change of the particles is also in agreement with the measured director field, where upon the nematic to isotropic transition the shells contract along the nematic long axis and expand in the perpendicular dimensions. The conformational change can yield a rise of hydrostatic pressure on the internal core. Due to this we create an exit possibility for the core by poking the shell elastomers with a sharp capillary tip. The actuation of the shell triggered by temperature change thus reversibly pumps the core liquid into and out of the shell (Fig. 3.8 c). The responsive time is within a second. The hollow shells exhibiting the unique heart-like movement are considered as potential micropumps for being utilized in microfluidic techniques.

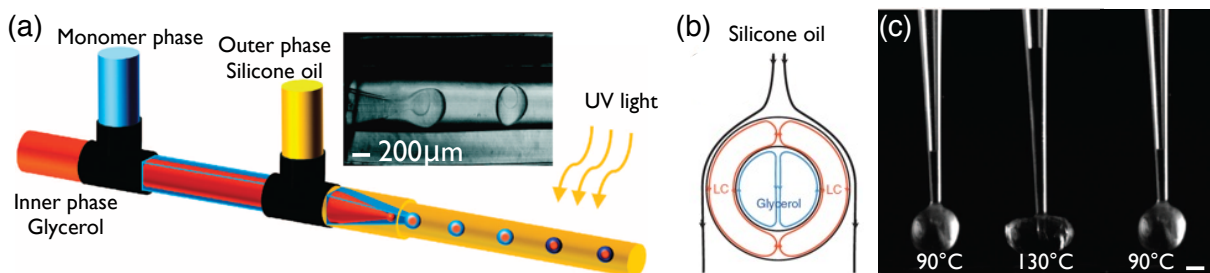


**Figure 3.8** (a) Production of the core-shell liquid crystalline elastomers in our co-flow microfluidic device. (b) Sketch of the internal flow of the monomer mixture and the glycerol core. The bipolar orientation may be driven by the flow profiles of the shell and the core volumes. (c) Core-shell actuating behavior at the elastomeric nematic ( $90^{\circ}\text{C}$ ) to isotropic ( $130^{\circ}\text{C}$ ) transition exhibiting a pumping effect on the inner core with the insertion of a capillary tip. (Scale bar= $100\ \mu\text{m}$ )

## 4 Summary and outlook

This thesis presented experimental studies of small molecular nematic, smectic and elastomeric liquid crystalline shells fabricated by glass capillary microfluidic devices. The devices were incorporated with heating facilities allowing for our work dealing with shell formation at elevated temperatures.

In the introductory sections I introduced the background of the research field concerning liquid crystals in shell morphology and the approaches to the optical analyses of the textures in liquid crystal shells, which were relevant to the new results produced in this thesis work. For low molar mass liquid crystal shells we conducted textural analyses of the nematic to SmA transition in shells under planar and hybrid alignment, the SmA to SmC transition in shells under homeotropic alignment, and a peculiar orientation transformation from planar to homeotropic alignment upon temperature change in shells stabilized by the polymeric surfactant F127.

Compared to bulk droplets, shells possess a significant reduction of volume in the spherical form, therefore liquid crystal shells exhibit defect configurations that are distinct from those of freely floating droplets. While SmA droplets under planar alignment develop irregular focal conic domains, thin SmA shells form a unique buckling texture due to layer undulation in order to solve the layer dilation imposed by the curvature strain. For the results regarding the introduction of hybrid alignment, which is not achievable in droplets, the shells are tiled with nearly toroidal domains. The domain size can be tuned by changing the shell thickness.

The microfluidic production of liquid crystal shells was further exploited for the production of well-aligned elastomeric liquid crystals. Though the alignment was hardly distinguished in the polarizing microscopy due to strong scattering from the polymer network, the bipolar orientation was confirmed by X-ray measurements. Undergoing the phase transition from the supercooled nematic to the isotropic phase, the elastomer shells were conformationally contracted along the director field and expanded perpendicular to it due to the loss of the orientational order. Under heating-cooling cycles the actuation reversibly exerted pressure on the inner liquid core, where the shells acted like heart-like micropumps.

Beside the above mentioned results, this thesis work also poses questions, namely regarding the complex phenomena involving the alignment transformation under the influence of F127 and the complexity of the molecular order in SmC shells, further investigations of which are currently on going.

For practical uses of small molecular liquid crystalline shells we find that the stabilization of the double emulsion is a crucial issue. The shells are water permeable, which may be one of the reasons for the rupture of the shells produced using aqueous solution as the interior and exterior phase. A proposed solution would be using oil phase as the inner core, creating a barrier for the interflow through the shell. Another intriguing strategy would be coating liquid crystals on actuatable hydrogels as the core material, where the hydration of the core may cause the change of shell thickness thus flexibly altering the symmetry of liquid crystal defect configurations without confronting the risk of shell rupture.

## References

- [1] (a) F. Reinitzer, *Monatshefte für Chemie*, 1888, **9**, 421; (b) T. Sluckin, D. Dunmur and H. Stegemeyer, *Crystals That Flow*, Taylor & Francis, London & New York, 2004, p. Paper A1.
- [2] (a) O. Lehmann, *Zeitschrift für Physikalische Chemie*, 1889, **4**, 462; (b) T. Sluckin, D. Dunmur and H. Stegemeyer, *Crystals That Flow*, Taylor & Francis, London & New York, 2004, p. Paper A2.
- [3] (a) G. Friedel, *Annales de Physique (Paris)*, 1922, **18**, 273–474; (b) T. Sluckin, D. Dunmur and H. Stegemeyer, *Crystals That Flow*, Taylor & Francis, London & New York, 2004, p. Paper B1.
- [4] S. Chandrasekhar, B. Sadashiva and K. Suresh, *Pramana*, 1977, **9**, 471.
- [5] O. Hewwmann-Schonherr, J. Wendorf, H. Ringsdorf and P. Tschirner, *Makromol. Chem. Rap. Commun.*, 1986, **7**, 791.
- [6] T. Niori, T. Sekine, J. Watanabe, T. Furukawa and H. Takezoe, *J. Mater. Chem.*, 1996, **6**, 1231.
- [7] (a) R. Virchow, *Virchows Archiv*, 1854, **6**, 562–572; (b) C. Mettenheimer, *Correspondenz- Blatt des Vereins für gemeinschaftliche Arbeiten zur Förderung der wissenschaftlichen Heilkunde*, 1857, **24**, 331.
- [8] O. Lehmann, *Flüssige Kristalle*, Wilhelm Engelmann, Leipzig, 1904.
- [9] N. Nakashima, S. Asakuma and T. Kunitake, *J. Am. Chem. Soc.*, 1985, **107**, 509.
- [10] T. C. Lubensky and J. Prost, *J. Phys. II France*, 1992, **2**, 371–382.
- [11] D. Nelson, *Nano Lett.*, 2002, **2**, 1125–1129.
- [12] A. Fernandez-Nieves, V. Vitelli, A. Utada, D. Link, M. Mrquez, D. Nelson and D. Weitz, *Phys. Rev. Lett.*, 2007, **99**, 157801.
- [13] M. Bates, *J. Chem. Phys.*, 2008, **128**, 104707.
- [14] H. Shin, M. Bowick and X. Xing, *Phys. Rev. Lett.*, 2008, **101**, 37802.
- [15] T. Lopez-Leon, V. Koning, K. Devaiah, V. Vitelli and A. Fernandez-Nieves, *Nat. Phys.*, 2011, **7**, 391–394.
- [16] D. Sec, T. Lopez-Leon, M. Nobili, C. Blanc, A. Fernandez-Nieves, M. Ravnik and S. umer, *Phys. Rev. E*, 2012, **86**, .
- [17] V. Koning, T. Lopez-Leon, A. Fernandez-Nieves and V. Vitelli, *Soft Matter*, 2013, **9**, 4993.
- [18] (a) P. Oswald and P. Pieranski, *Smectic and Columnar Liquid Crystals*, Taylor & Francis, Boca Raton, 2005, p. Chap. 8; (b) P. Oswald, *J. Phys. France*, 1987, **48**, 897–902.
- [19] F. Mueller and R. Stannarius, *Liquid Crystals*, 2009, **36**, 133–145.
- [20] R. Pinol, L. Jia, F. Gubellini, D. Levy, P.-A. Albouy, P. Keller, A. Cao and M.-H. Li, *Macromolecules*, 2007, **40**, 5625–5627.
- [21] L. Jia, A. Cao, D. Levy, B. Xu, P.-A. Albouy, X. Xing, M. J. Bowick and M.-H. Li, *Soft Matter*, 2009, **5**, 3446.
- [22] X. Xing, *J. Stat. Phys.*, 2009, **134**, 487–536.
- [23] X. Xing, H. Shin, M. Bowick, Z. Yao, L. Jia and M. Li, *Proc. Natl. Acad. Sci. U.S.A.*, 2012, **109**, 5202.
- [24] Y. Uchida, Y. Takanishi and J. Yamamoto, *Adv. Mater.*, 2013, Advance Article.
- [25] E. Fleischmann, H. Liang, N. Kapernaum, F. Giesselmann, J. Lagerwall and R. Zentel, *Nat. Commun.*, 2012, **3**, 1178.

- [26] G. Whitesides, *Lab Chip*, 2011, **11**, 191–193.
- [27] R. Shah, H. Shum, A. Rowat, D. Lee, J. Agresti, A. Utada, L. Chu, J. Kim, A. Fernandez-Nieves, C. Martinez and D. Weitz, *Mater. Today*, 2008, **11**, 18–27.
- [28] A. Abate and D. Weitz, *Small*, 2009, **5**, 2030–2032.
- [29] A. Utada, E. Lorenceau, D. Link, P. Kaplan, H. Stone and D. Weitz, *Science*, 2005, **308**, 537–541.
- [30] C. Ohm, C. Serra and R. Zentel, *Adv. Mater.*, 2009, **21**, 4859–4862.
- [31] (a) P.-G. de Gennes, *Phys. Lett. A*, 1969, **28**, 725; (b) P.-G. de Gennes, *C. R. Acad. Sci. Ser. B*, 1975, **281**, 101.
- [32] E. Fleischmann and R. Zentel, *Angew. Chem.*, 2013, in preparation.
- [33] D. Demus, *Textures of liquid crystals*, Verlag Chemie, Weinheim, 1978.
- [34] O. Lavrentovich, *Sov. Phys. JETP*, 1986, **64**, 984–990.
- [35] (a) G. Volovic and O. Lavrentovich, *Sov. Phys. JETP*, 1983, **58**, 1159–1166; (b) H. Poincaré, *J. Math. Pures Appl.*, 1885, **1**, 167.
- [36] C. Blanc and M. Kleman, *Eur. Phys. J. E*, 2001, **4**, 241–251.
- [37] C. Meyer, L. Le, Cunff, M. Belloul and G. Foyart, *Materials*, 2009, **2**, 499–513.
- [38] S. Sivakumar, K. Wark, J. Gupta, N. Abbott and F. Caruso, *Adv. Funct. Mater.*, 2009, **19**, 2260–2265.
- [39] T. Bera and J. Fang, *Langmuir*, 2013, **29**, 387–392.
- [40] M. Kinsinger, M. Buck, N. Abbott and D. Lynn, *Langmuir*, 2010, **26**, 10234–10242.
- [41] V. Alino, P. Sim, W. Choy, A. Fraser and K. Yang, *Langmuir*, 2012, **28**, 17571–17577.
- [42] I. Lin, D. Miller, P. Bertics, C. Murphy, J. de Pablo and N. Abbott, *Science*, 2011, **332**, 1297–1300.
- [43] A. Fernandez-Nieves, D. Link, M. Mrquez and D. Weitz, *Phys. Rev. Lett.*, 2007, **98**, 87801.
- [44] T. Lopez-Leon and A. Fernandez-Nieves, *Phys. Rev. E*, 2009, **79**, 021707.
- [45] T. Lopez-Leon, M. Bates and A. Fernandez-Nieves, *Phys. Rev. E*, 2012, **86**, .
- [46] G. Whitesides, *Nature*, 2006, **442**, 368–373.
- [47] E. J. Maxwell, A. D. Mazzeo and G. M. Whitesides, *MRS Bull.*, 2013, **38**, 309–314.
- [48] A. Gánán Calvo and J. Gordillo, *Phys. Rev. Lett.*, 2001, **87**, 274501.
- [49] W. Wang, R. Xie, X. Ju, T. Luo, L. Liu, D. Weitz and L. Chu, *Lab Chip*, 2011, **11**, 1587–1592.
- [50] H. Shum, Y. Zhao, S. Kim and D. Weitz, *Angew. Chem. Int. Edit.*, 2011, **50**, 1648–1651.
- [51] L. L. A. Adams, T. E. Kodger, S.-H. Kim, H. C. Shum, T. Franke and D. A. Weitz, *Soft Matter*, 2012, **8**, 10719.
- [52] A. Rotem, A. Abate, A. Utada, V. Van Steijn and D. Weitz, *Lab Chip*, 2012, **12**, 4263–4268.
- [53] Y. Chiu, S. Cho, Z. Mei, V. Lien, T. Wu and Y. Lo, *Lab Chip*, 2013, **13**, 1803–1809.
- [54] M. Kleman and O. Laverentovich, *Soft Matter Physics: An Introduction*, Springer, New York, 2002.
- [55] B. Zappone and E. Lacaze, *Phys. Rev. E*, 2008, **78**, 061704.
- [56] Y. Kim, D. Yoon, H. Jeong, O. Lavrentovich and H. Jung, *Adv. Funct. Mater.*, 2011, **21**, 610–627.
- [57] P. Cladis and S. Torza, *J. Appl. Phys.*, 1975, **46**, 584–599.
- [58] M. A. Gharbi, D. Sec, T. Lopez-Leon, M. Nobili, M. Ravnik, S. Zümer and C. Blanc, *Soft Matter*, 2013, **9**, 6911–6920.



# Publications



PAPER 1.

**NEMATIC-SMECTIC TRANSITION UNDER CONFINEMENT IN LIQUID CRYSTALLINE COLLOIDAL SHELLS**

Hsin-Ling Liang, Stefan Schymura, Per Rudquist and Jan Lagerwall  
*Phys. Rev. Lett.*, **106**, 247801 (2011)



PAPER 2.

**TOWARDS TUNABLE DEFECT ARRANGEMENTS IN SMECTIC LIQUID CRYSTAL SHELLS UTILIZING THE NEMATIC–SMECTIC TRANSITION IN HYBRID-ALIGNED GEOMETRIES**

Hsin-Ling Liang, Rudolf Zentel, Per Rudquist and Jan Lagerwall  
*Soft Matter*, **8**, 5433 (2012)



PAPER 3.

**LIQUID CRYSTALS IN NOVEL GEOMETRIES PREPARED BY MICROFLU-  
IDICS AND ELECTROSPINNING**

Hsin-Ling Liang, Eva Enz, Guisy Scalia and Jan Lagerwall  
*Mol. Cryst. Liq. Cryst.*, **549**, 6977 (2011)



PAPER 4.

**TUNING THE DEFECT CONFIGURATIONS IN NEMATIC AND SMECTIC LIQUID CRYSTALLINE SHELLS**

Hsin-Ling Liang, JungHyun Noh, Rudolf Zentel, Per Rudquist and Jan P. F. Lagerwall  
*Phil. Trans. R. Soc. A*, **371**, 20120258 (2013)



PAPER 5.

**TOWARDS MICROMETER SIZED CORE-SHELL ACTUATORS FROM  
LIQUID CRYSTALLINE ELASTOMERS BY A CONTINUOUS FLOW SYN-  
THESIS**

Eva-Kirstina Fleischmann, Hsin-Ling Liang, Jan Lagerwall and Rudolf Zentel  
*Proc. of SPIE*, **8729**, 82790M-1 (2012)



PAPER 6.

**ONE-PIECE MICROPUMPS FROM LIQUID CRYSTALLINE CORE-SHELL PARTICLES**

Eva-Kirstina Fleischmann, Hsin-Ling Liang, Nadia Kapernaum, Frank Giesselmann, Jan Lagerwall and Rudolf Zentel

*Nat. Commun.*, DOI: [10.1038/ncomms2193](https://doi.org/10.1038/ncomms2193) (2012)



## ACKNOWLEDGEMENTS

It feels like yesterday, when I was riding a bus in Seoul early this year, anxious about my writing progress, and yet I have been here at the final page. In this journey I am especially appreciative of the book “*Crystals that flow*”, for its collection of classic papers was as a time machine leading me back to relearn liquid crystals from the great discoverers.

Coming to Germany for my doctoral studies was a beautiful course of life. First and foremost, I must thank Prof. Jan Lagerwall, who was with me to apply for the DAAD scholarship and has taken me under his wings, teaching me not only the science of liquid crystals from the basics with the utmost patience, but also the spirit of humility in his own deeds of being a great scientist. In my every unsuccessful attempt, he held all positive encouragement for me to have faith in myself.

I am sincerely grateful to Prof. Rudolf Zentel. I am glad to have taken his advice to move to Mainz instead of under remote supervision when facing Jan’s moving to Korea. He was wise enough to know that a doctoral student is better off with an advisor and colleagues around. He provided me a resourceful environment to continue carrying out my research project, and brought me into the IRTG family that allowed me to visit Korea. For every request regarding my new status, he found a solution.

I am deeply indebted to Eva Fleischmann, my dear friend and partner on the battlefield of Yellow Lightroom, who always generously lent her considerate hand whenever I needed help, and gave me the most delightful and unforgettable teamwork on LCE shells.

I have benefitted a lot from Prof. Per Rudquist and his brilliant mind in analyzing the director field in 3D shells. My great appreciation also goes to Prof. Ralf Stannarius for valuable discussions in smectic C shells and kindly being my reference contact for my scholarship. I am very lucky to have excellent collaborators – Kirsten Harth, who generously shared her in-depth knowledge of smectic phases; JungHyun Noh, for the great time working together on microfluidics and for her hospitality during my visit in Korea.

Furthermore, I am very fortunate to have worked with two research groups, from where I got enormous help and support – at my time in Halle, I owe deep thankfulness to Stefan Schymura, Eva Enz, Sarah Dölle and Martin Kühnast for creating an open, fun and stimulating atmosphere for scientific discussions, as well as giving their best to acquaint me with my new life abroad. Special thanks to Stefan, my forerunner on the microfluidic experiments, without whose precedent experience I would have taken longer time before reaching the core of the project. In Mainz, I was surrounded by knowledgeable and friendly people who welcomed me as a new member. In particular, I thank Lutz Nuhn, who introduced me to silanization processes, which improved my setups a great deal; Annette Kelsch and Linda Kircher, who patiently spoke German with me to keep my language skill from going completely *kaputt*; Mareli Allmeroth and Mirjam Hemmelmann, for their companionship even after their leaving.

My heartfelt thanks to Prof. Giusy Scalia, who very dearly cares about my research progress and lifts me up when I feel lost. Her passion for science and sparkle in the eye when talking about new ideas are soul-stirring for me as a female researcher. Time is always too short for many enjoyable discussions with her on various topics.

My profound gratitude to Lili Jia, Amira Apaza, Yi-Ting Tu, Wen-Min Hsieh, Chen-Chia Wei and Chung-Lan Lin for their presence and friendship that made the completion of my studies in a foreign country possible. Finally, I want to dedicate my accomplishment to my grandparents and parents, for this work would not be possible without their unconditional love and tolerance to my absence around them.

